JAERI-M

6761

SPECTROSCOPIC INVESTIGATIONS OF THE VACUUM ULTRA-VIOLET EMISSION IN A NORMAL-INCIDENCE REGION FROM JFT-2 TOKAMAK DISCHARGE

(B_t=9 kGauss and I_p =76 kAmp)

October 1976

S. KASAI, A. FUNAHASHI, T. TAZIMA*,

and Y. NAKAMURA*

日本原子力研究所

Japan Atomic Energy Research Institute

JAERI - M 6761

Spectroscopic Investigations of the Vacuum Ultra-violet Emission in a Normal-incidence Region from JFT-2 Tokamak Discharge (B_t = 9 kGauss and I_p = 76 kAmp)

Satoshi KASAI, Akimasa FUNAHASHI, Teruhiko TAZIMA+,

and Yukiharu NAKAMURA*

Division of Thermonuclear Fusion Research, Tokai, JAERI

(Received September 30, 1976)

Spectroscopic investigations have been performed in the wavelength range of 600 to 2300 Å on a JFT-2 plasma with peak plasma current 76 kAmp, toroidal magnetic field 9 kGauss, and electron and ion temperature 300--350 eV and 200 eV respectively. Time-histories were measured of spectral lines radiating from oxygen and carbon impurities. The radial profiles of CV(2270.9 Å) and OVII(1623.3 Å) lines were measured, which showed the spatial distributions with cylindrical shells. The experimental results are compared with the theoretical ones calculated numerically by using a plasma model based on the coronal equilibrium and particle loss due to the diffusion process. Time-variation of the electron temperature during the initial phase of discharge are estimated from the measured time-histories of impurity lines, and the peak electron temperature agrees with that determined from measurements of the ruby laser scattering. The spatial distributions of CV and OVII lines are reasonably explained by the inward-diffusion flux and the diffusion flux, which is several ten times of Pfirsch-Schlüter's one.

+ Division of Large Tokamak Development, Tokai, JAERI.

* One leave from Sumitomo Heavy Industries, LTD.

JAERI－M 6761

JFT－2トカマクプラズマ(B_t = 9 kGauss, I_p = 76 kAmp)からの真空紫外直入射域放射の分光研究

日本原子力研究所東海研究所核融合研究部

河西　敏・船橋　昭昌
田島　輝彦[+]・中村　幸治[*]

(1976年9月30日受理)

JFT－2プラズマについて分光学的研究を600から2300Å波長域において行った。実験条件は，トロイダル磁場9kG，最大プラズマ電流76kA，最大電子およびイオン温度は300～350 eVである。酸素および炭素不純物から輻射されるスペクトル線の時間経過を測定した。またCV（2270.9Å）およびOVII（1623.3Å）線の半径方向分布の測定から，これらスペクトル線は円筒状シェル構造分布をしていることが確められた。この実験結果とコロナ平衡および粒子拡散損失を考慮したプラズマモデルを使って数値解析的に得られる理論的結果との比較を行った。不純物線の時間経過から電子温度の初期時間変化について評価し，ルビーレーザ散乱測定から決められた電子温度との一致を見た。更にCVおよびOVII線の空間分布は，不純物の内向き拡散束および数十倍のPfirsch－Schlüter拡散束によって説明できた。

+) 日本原子力研究所東海研究所　大型トカマク開発部

*) 外来研究員：住友重機（株）

CONTENTS

I. INTRODUCTION

The present paper is describing (i) the estimation of time-variation of electron temperature in an initial phase of a discharge from time-histories of spectral lines emitted and (ii) the transportation of impurity-ions from radial profiles of spectral intensities observed in a JFT-2 tokamak-plasma. Measurements were carried out under the following conditions, toroidal magnetic field $B_t = 9$ kGauss, peak plasma current $I_p = 76$ kAmp, filling pressure of hydrogen gas $P = 3.2 \times 10^{-4}$ torr and a radius of aperture limiter $a = 25$ cm.[1,2]

(i) The estimation of electron temperature from time-histories of impurity-lines has been attempted in some plasma devices. Goldman and Kilb[3] determined electron temperatures during an early compression stage of a θ-pinch plasma only by considering ionization and recombination processes from the times of appearance and peak intensity of carbon and oxygen lines in their various stages of ionization. Hobbs et al. estimated the electron temperature in the Zata device by this method. However in the case of a tokamak plasma, the particle loss becomes important as well as ionization and recombination processes, and then a rate of the loss must be taken into account on the estimation of electron temperature from the time history method. In the present paper we consider the particle loss and the neutral impurity flux and evaluate the electron temperature in the initial phase of a JFT-2 discharge. Recently for a TFR tokamak plasma,[5,6,7] the similar method described in the present paper was used to determine the averaged electron temperature at the early time. Ohasa et al.[8] also determined the electron temperature in the JIPP-Ib stellarator device from the times of appearance of impurity lines. The present work have been independently performed in order to examine the initial rise of electron temperature in the JFT-2 device.

(ii) It has been discussed the problems of transportation for impurities in tokamak plasmas in experimental and theoretical works. Vershkov and Mirnov[9] pointed out that there existed the diffusion of impurity towards the plasma center and that the impurity accumulated in the central region of the plasma.[10] Connor,[11] Tsuda and Tanaka,[12] and Rutherford[13] indicated theoretically the possibility of an accumulation of impurity. However in ST[14,15,16,17] and TFR[5,18] tokamak plasmas, it was concluded that there did not exist large diffusions of impurities inwards in a plasma column, or very substantial accumulations of impurities. Recently Cohen et al.[19] reported that in ATC plasmas the impurity transport was neoclassical (collisional)

and included an inward diffusion. In the present paper we compare the experimental distributions of impurity-lines with those numerically calculated[20] by considering the ordinary diffusion and the inward diffusion of impurity-ions.

In the present investigations, we are not able to avoid the difficulty in quantitative discussions because absolutely calibrated measurements have not been performed. The diagnostic apparatus used in the present experiments are described in Section Ⅱ. Experimental results for time history and spatial distribution of impurity lines are described in Section Ⅲ, and results of numerical calculations in Section Ⅳ.

II. DIAGNOSTIC APPARATUS

Figure 1 shows a plan view of the JFT-2 device and diagnostic apparatus for measurements of the JFT-2 plasmas.[1,2] Measurements are mainly performed through observation boxes named b_1, b_3 and b_4. A molybdeneum aperture limiter with its diameter of 50 cm is inserted in the b_2 box. Rail plates of the dynamic limiter are installed at top and bottom of the b_3 box. However, the dynamic limiter is not operating in the experiments described in the present report, and the distance of these plates is fixed to be 51 cm.

Electron temperatures are determined from measurements of scattered intensities in ruby-laser lights or soft X-ray spectra. Electron densities are vertically measured with a 4-mm microwave interferometer attached at the b_4 box. A normal-incidence, vacuum ultra-violet (v.u-v.) monochrometer is horizontally connected at the b_3 box. The monochrometer observes spectral intensities integrated along the major-radius direction. The v.u-v. monochrometer has an optical system with a Robin-Vodar mounting and its focal length of 50 cm. A concave grating (1200 lines/mm) coated with M_gF_2 and blazed at 1500 Å is used for the monochrometer. The wavelength resolution has been examined to be about 0.5 Å for a mercury line of 3131.7 Å. A photomultiplier (RCA6810A) with a scintillator (sodium salicylate) is adopted as a photoelectric detector. Photographic measurements are also performed with the monochrometer. The Eastman Kodak SWR emulsions produced commercially are used for photographic measurements. A vacuum system of the monochrometer includes a 4-inch oil-diffusion pump with a cold trap of liquid nitrogen, mechanical booster and oil rotary pumps. The pressure in the monochrometer is kept below 2×10^{-5} torr in all measurements.

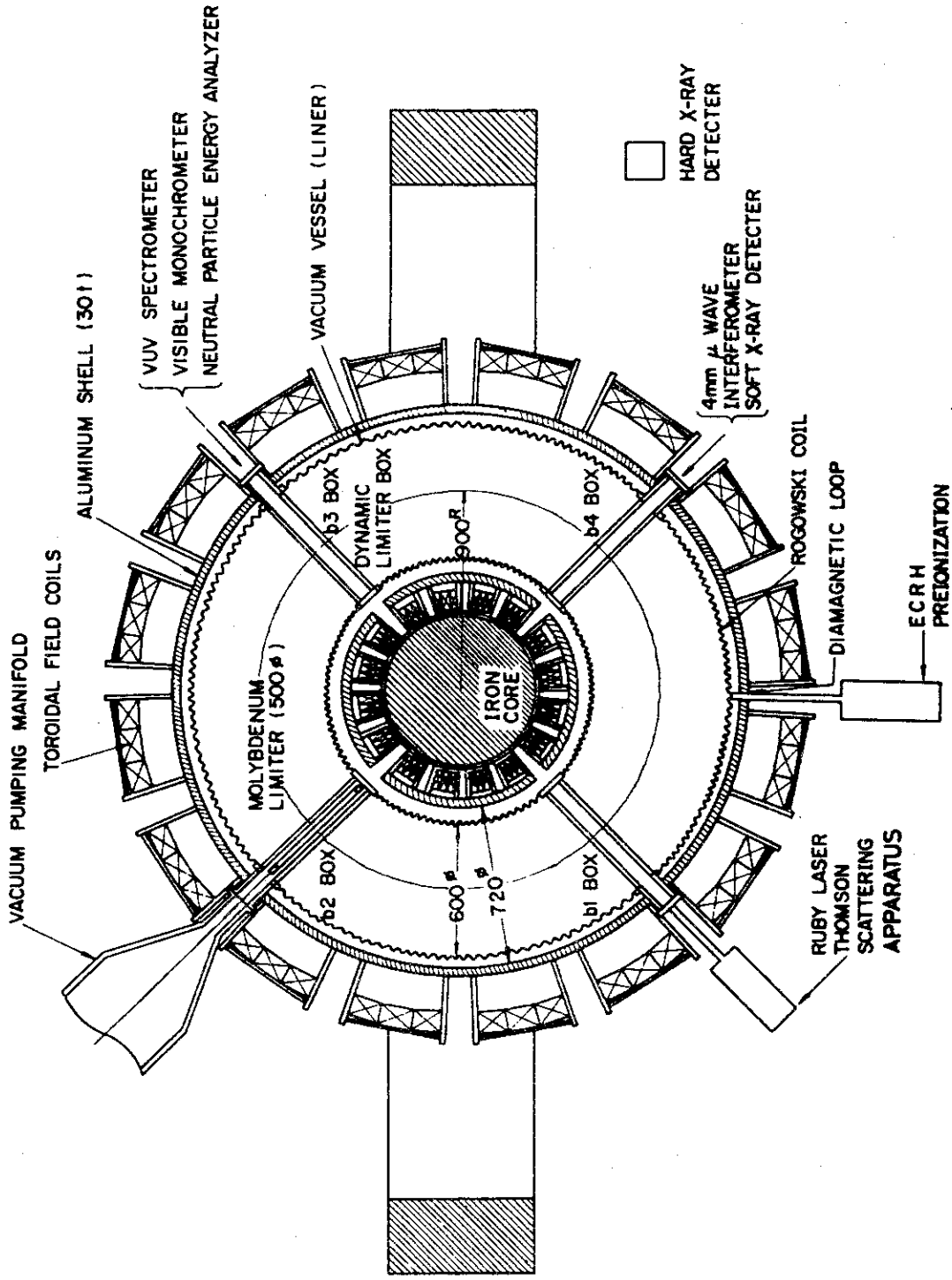

Fig. 1 Plan view of the JFT-2 device and diagnostic instruments.

III. EXPERIMENTAL RESULTS

1. Plasma parameters

Measurements are made on the JFT-2 plasma obtained under an operating condition which was previously reported in IAEA Tokyo Conference.[1)]

The major and minor radii of the plasma are 90 cm and 25 cm respectively. The strength of toroidal magnetic field is 9 kGauss. The vacuum vessel of the JFT-2 device is filled with the hydrogen gas at a pressure of 3.2×10^{-4} torr through a gas injection system of continuous-flowing admission.

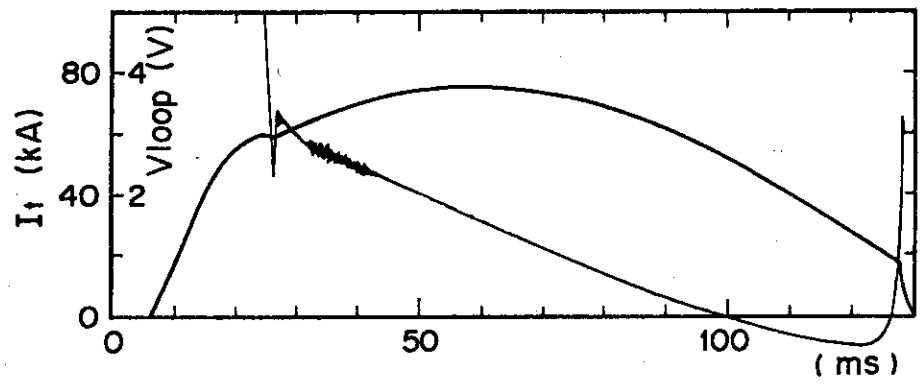

(a)

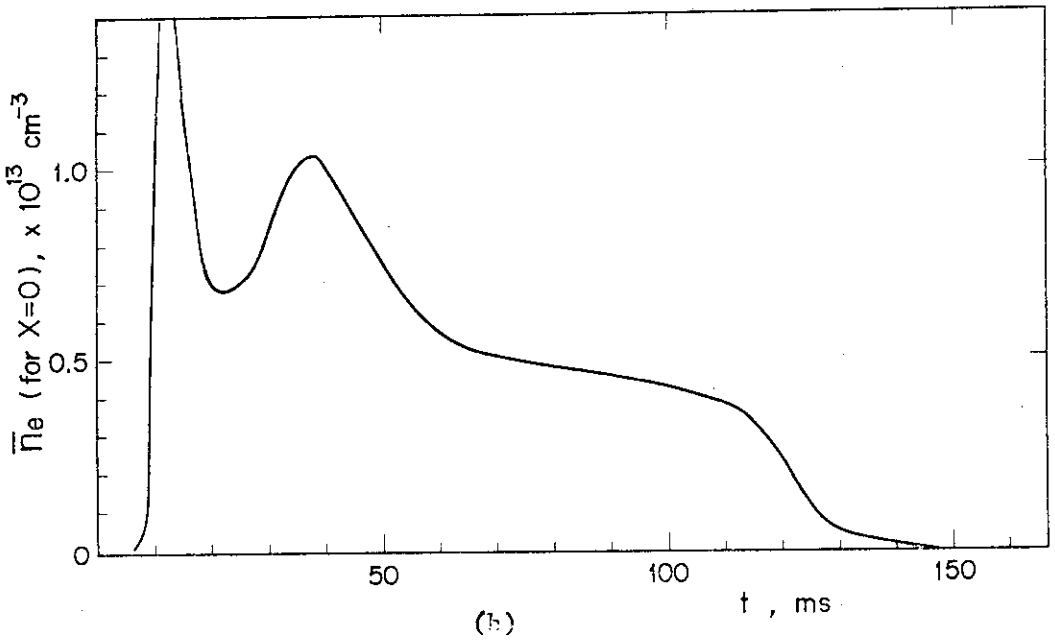

(b)

Fig. 2 Time-evolutions of the plasma current and loop voltage (a) and the averaged central electron density (b).

The plasma current is flowed in the direction opposite to the toroidal magnetic direction, and the time-evolution of the current is shown in Fig. 2(a). The peak value of the plasma current, which is about 76 kA, is realized at 60 msec. The average electron density $\bar{n}_e$ (solid curve) at 30 msec is plotted against the horizontal position X in Fig. 3. A radial profile $n_e(r)$ of the electron density is obtained by an inverse-transformation method and drawn by a broken line in the figure. The electron density at 30 msec has approximately a profile of the squared distribution $n_e(r) \propto [1 - (r/b)^2]$ with the minor radius b of the vacuum vessel (liner), although a small inward shift of a few cm is observed.

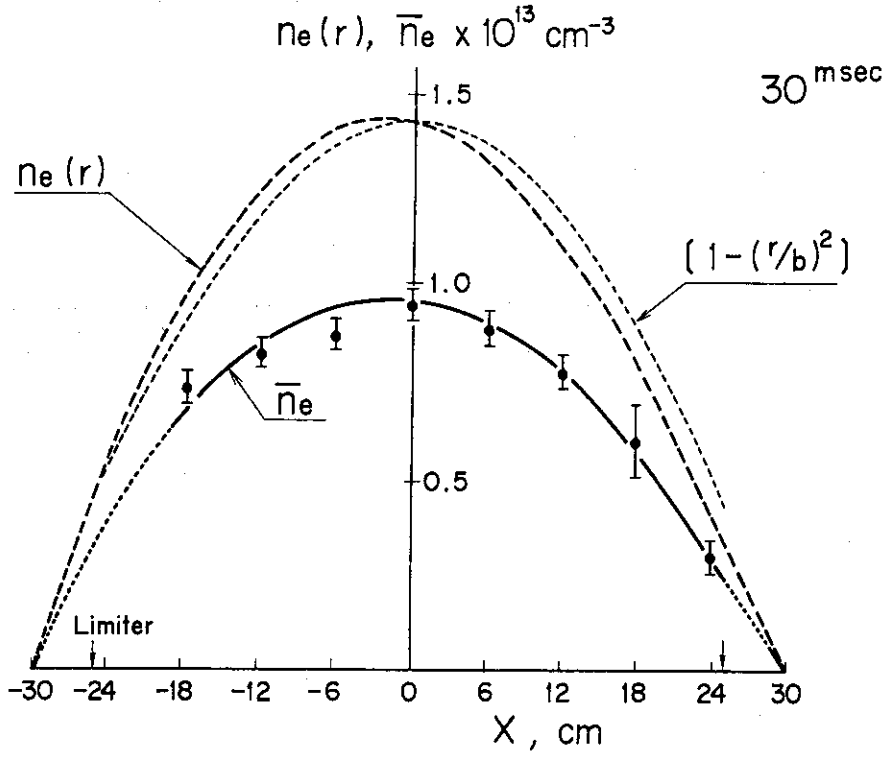

Fig. 3 Radial profile of the electron density at 30 msec.

2. Line identification

Spectrographic measurements are carried out under operating conditions of discharge cleanings, where the toroidal magnetic field and plasma current are rather small. An entrance slit is opened to be 10 μm or 20 μm. A C_aF_2 window inserted in front of the entrance slit is used to remove the second-order spectral lines for the measurements in the wavelength range from 1200 to 2000 Å.

Figures 4(a), 4(b) and 4(c) show spectral lines in the wavelength range from 1200 to 2000 Å obtained by scanning the spectra exposed on the film with a microphotometer. And spectral lines from 600 to 1200 Å are presented in Fig. 5. These data are obtained for plasma discharges of about 500 shots. Identified spectral lines are emitted from carbon, oxygen and nitrogen ions, which are similar to results in conventional tokamak devices, and metallic ions (F_e, C_r, N_i) which are constituent materials of the stainless-steel vacuum vessel. In Fig. 4, the spectral lines of CⅣ (1548.2 Å, 1550.8 Å) and S_iⅣ (1393.8 Å, 1402.8 Å), which are respectively lithium-like and sodium-lide and are resonance lines show the doublet spectra. The lines of CⅡ (1334.5 Å) and S_iⅡ (1526.7 Å) are also resonance ones. The lines from Fe, Cr and Ni assemble in the range from 1200 to 2000 Å, and the Fe-lines compose a multiplet spectrum which arises from a fine structure. The C_rV-lines of 1580 Å and 1592 Å are identified. However, oxygen, carbon and nitrogen ions are mainly observed in the wavelength range below 1200 Å, as shown in Fig. 5. Molybdenum lines can not be identified in the range from 600 to 2000 Å.

3. Time-history of spectral intensities of impurity lines

The time-histories of relative spectral intensities of impurity-gas lines and Lyman alpha line (L_α) are measured with the v.u.-v. monochrometer observing the plasma center in the major-radius direction. Figures 6(a) and 6(b) show typical oscilloscopic traces for L_α, CⅣ (1548.2 Å), CⅤ (2270.9 Å), OⅥ (1037.6 Å) and OⅦ (1623.3 Å) lines. The upper trace of the data corresponds to an initial stage of the discharge, and the low trace presents time-variations of each line during the whole discharge. Spectral lines of L_α, CⅣ and OⅣ lines are luminous strongly in an early time of the discharge. After about 20 msec, these intensities decrease rapidly and become extremely weak. It is found that from Fig. 6 that CⅤ and OⅦ ions with high ionization-potentials (392.1 eV and 739.1 eV respectively) begin to be observed after 20 msec. Figure 7 shows time-histories of intensities

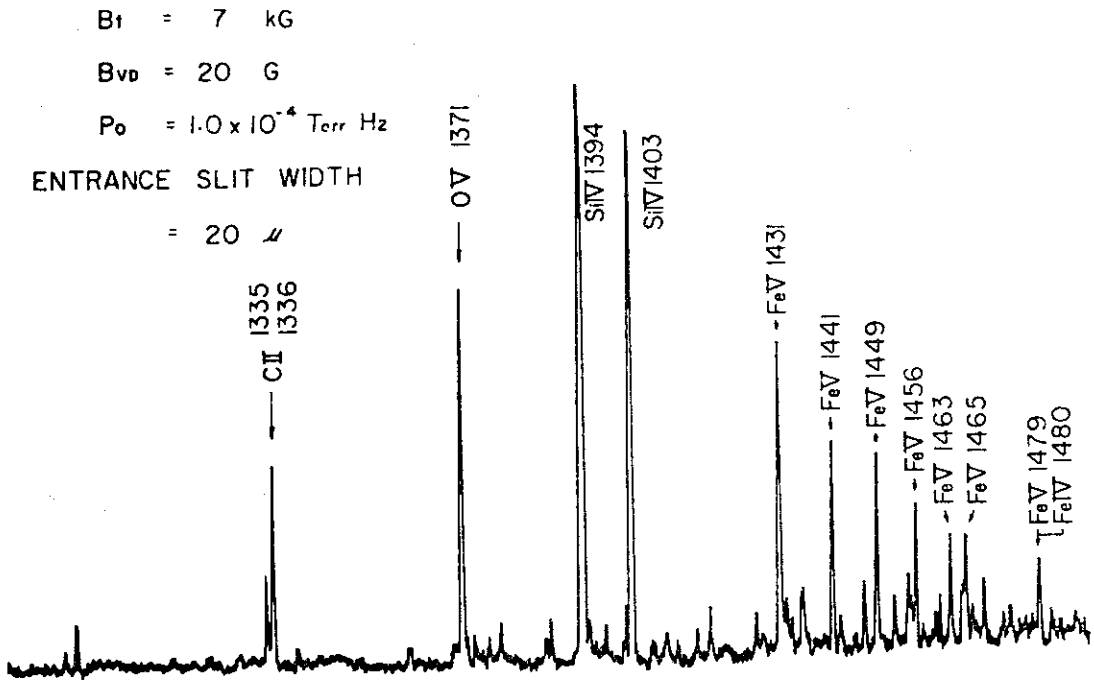
Bt = 7 kG
Bvd = 20 G
Po = 1.0 x 10⁻⁴ Torr H2
ENTRANCE SLIT WIDTH
= 20 μ
CII 1335 1336
OV 1371
SiIV 1394
SiIV 1403
FeV 1431
FeV 1441
FeV 1449
FeV 1456
FeV 1463
FeV 1465
FeV 1479
FeIV 1480

Fig. 4(a)

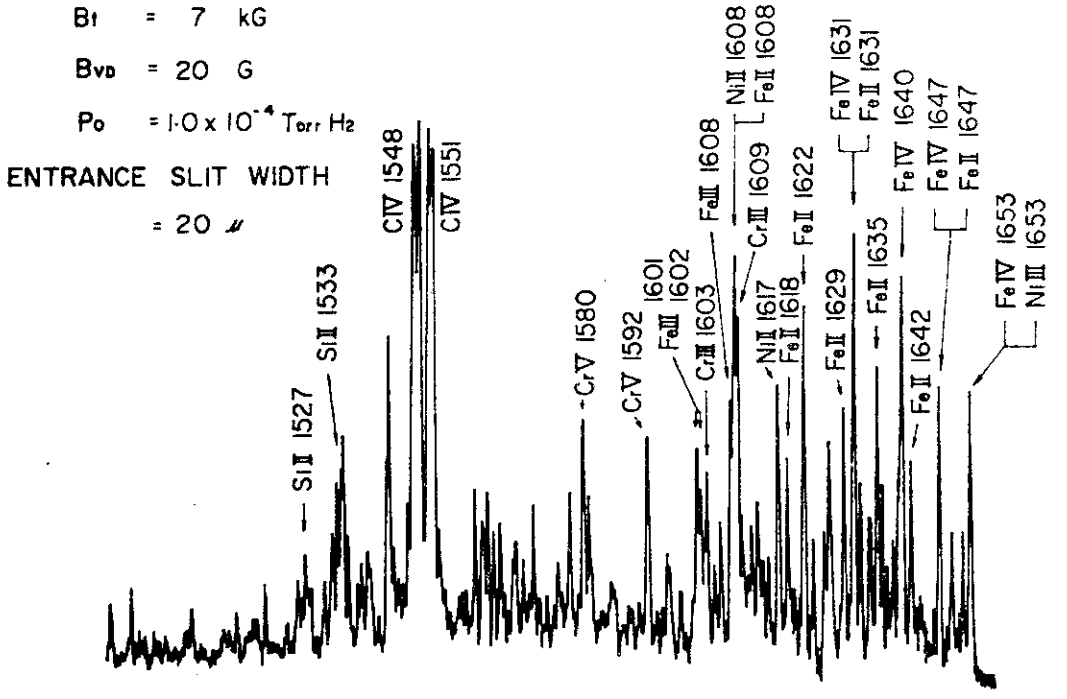
Bt = 7 kG
Bvd = 20 G
Po = 1.0 x 10⁻⁴ Torr H2
ENTRANCE SLIT WIDTH
= 20 μ
SiII 1527
SiII 1533
CIV 1548
CIV 1551
CrV 1580
CrV 1592
FeIII 1601
FeIII 1602
CrIII 1603
FeIII 1608
NiII 1608
FeII 1608
CrIII 1609
NiII 1617
FeII 1618
FeII 1622
FeII 1629
FeIV 1631
FeII 1631
FeII 1635
FeIV 1640
FeII 1642
FeIV 1647
FeII 1647
FeIV 1653
NiII 1653

Fig. 4(b)

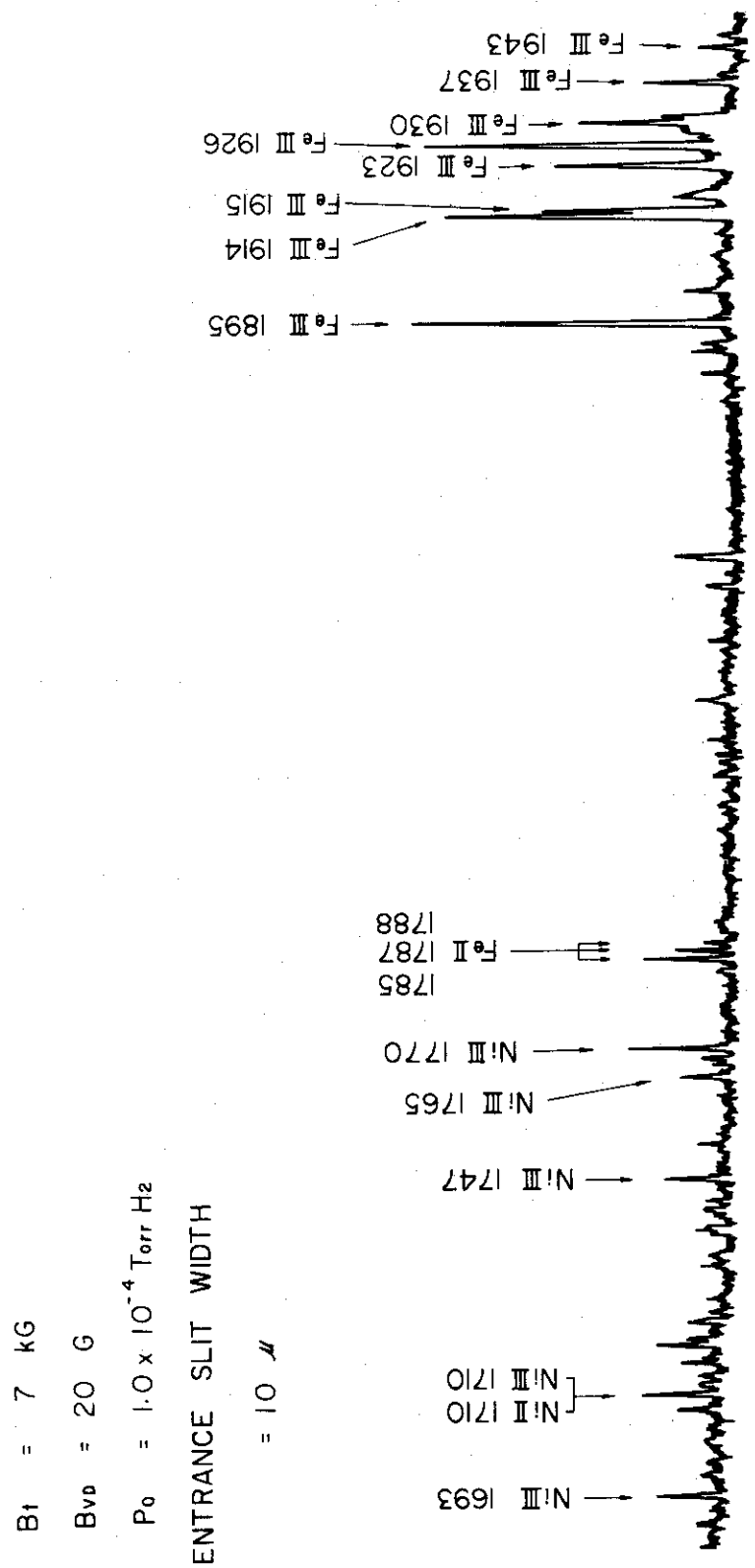

Fig. 4(c)

Fig. 4 Line identification in the wavelength range from 1200 to 2000 Å.

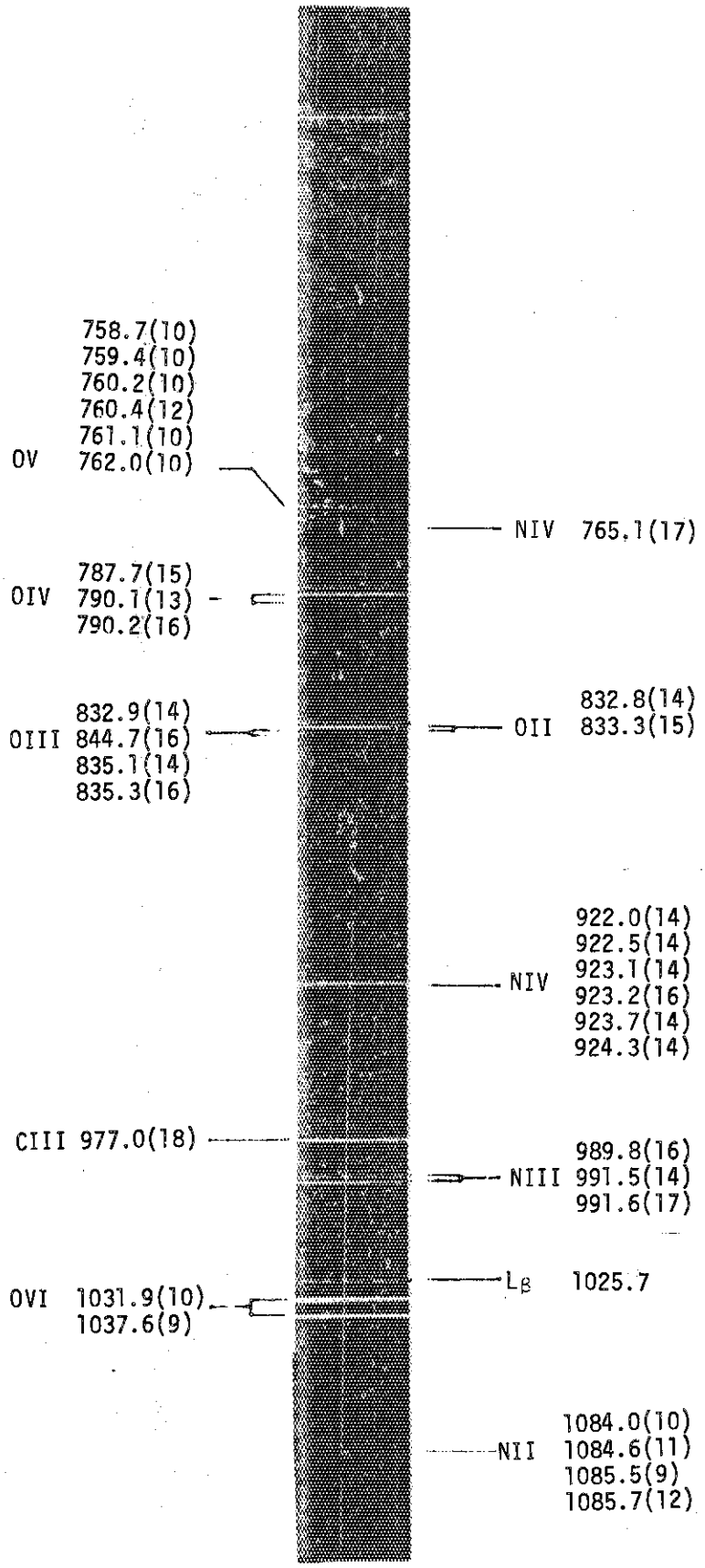

Fig. 5 Line identification in the wavelength range from 600 to 1200 Å.

L_α
5 ms/div, 200 mV/div
20 ms/div, 10 mV/div

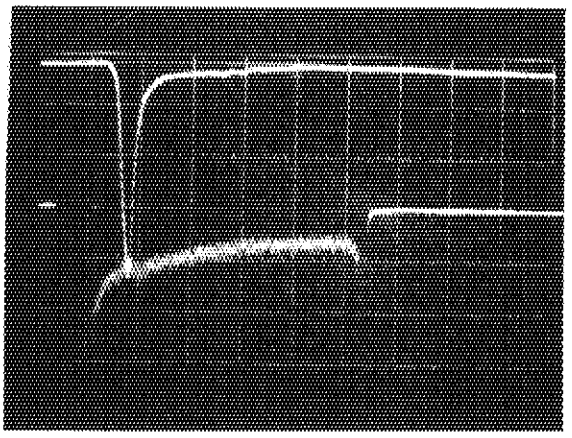

CIV(1548.2 Å)
5 ms/div, 500 mV/div
20 ms/div, 5 mV/div

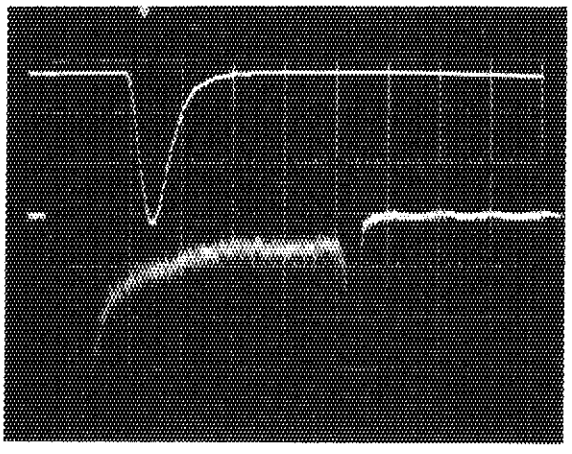

CV (2270.9 Å)
5 ms/div, 10 mV/div
20 ms/div, 5 mV/div

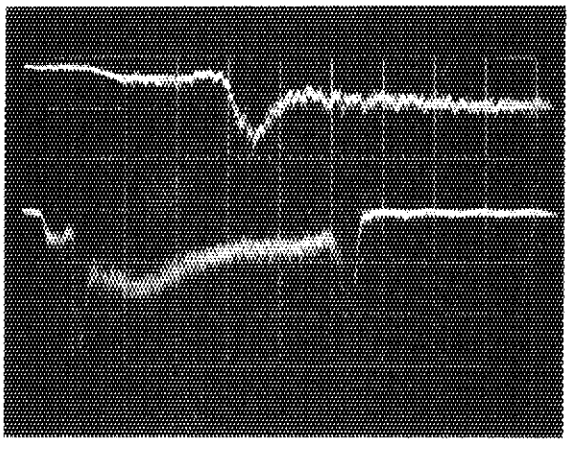

Fig. 6(a) Oscilloscopic traces for L_α, CIV(1548.2 Å) and CV(2270.9 Å) lines.

L_α
5 ms/div, 200 mV/div
20 ms/div, 10 mV/div

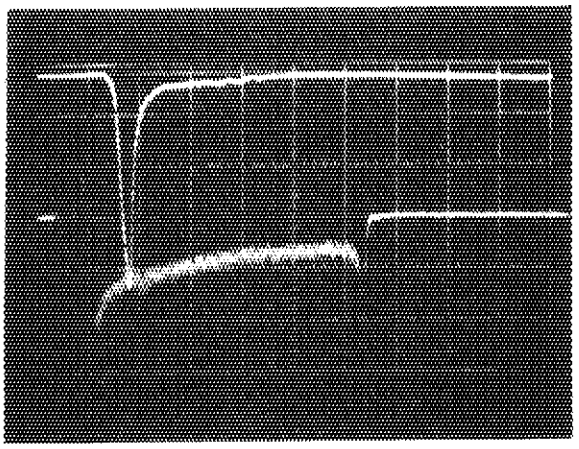

OVI (1037.6 Å)
5 ms/div, 100 mV/div
20 ms/div, 10 mV/div

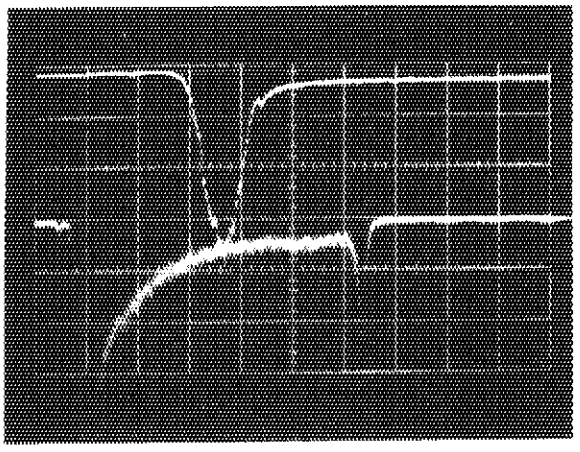

OVII (1623.3 Å)
5 ms/div, 10 mV/div
20 ms/div, 10 mV/div

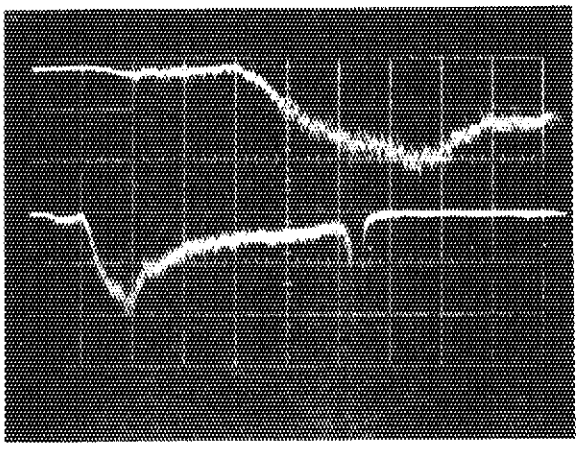

Fig. 6(b) Oscilloscopic traces for L_α, OVI(1037.6 Å) and CVII(1623.3 Å) lines.

normalized to peak intensities of individual lines. The time when the peak intensity is realized for each spectral line is different through its ionization potential. That is, the intensity peak of ion with the lower ionization-potential appears at the more early time and successively that with the higher ionization-potential appears. The ionization potentials (E_I) from the ground levels of individual ions and the excitation potentials (E_x) of observed spectral lines are also indicated in Fig. 7. The inset of the figure provides the time-evolutions of plasma current (I_p) and plasma loop voltage (V_{loop}).

4. Spetial distribution of spectral intensities of impurity lines

Spatial distributions of relative integrated intensities are measured by scanning the monochrometer vertically at the b_3 box, in order to obtain radial profiles of spectral lines. Figure 8 shows the spatial distribution of relative intensity I(Z) for the CV(2270.9 Å) line at 30 msec with the vertical position of an observing optical-path Z. Figure 9 shows the spatial distributions for OVII(1623.3 Å) line at 30 and 40 msec. At 30 msec the CV line has a peak intensity near Z = 8 cm and OVII line with the higher ionization potential has a peak intensity near the center of plasma column, but then at 40 msec the OVII line peaks near r = 8 cm, similarly to the CV line at 30 msec. These facts indicate that the electron temperature rises with the time between 30 and 40 msec.

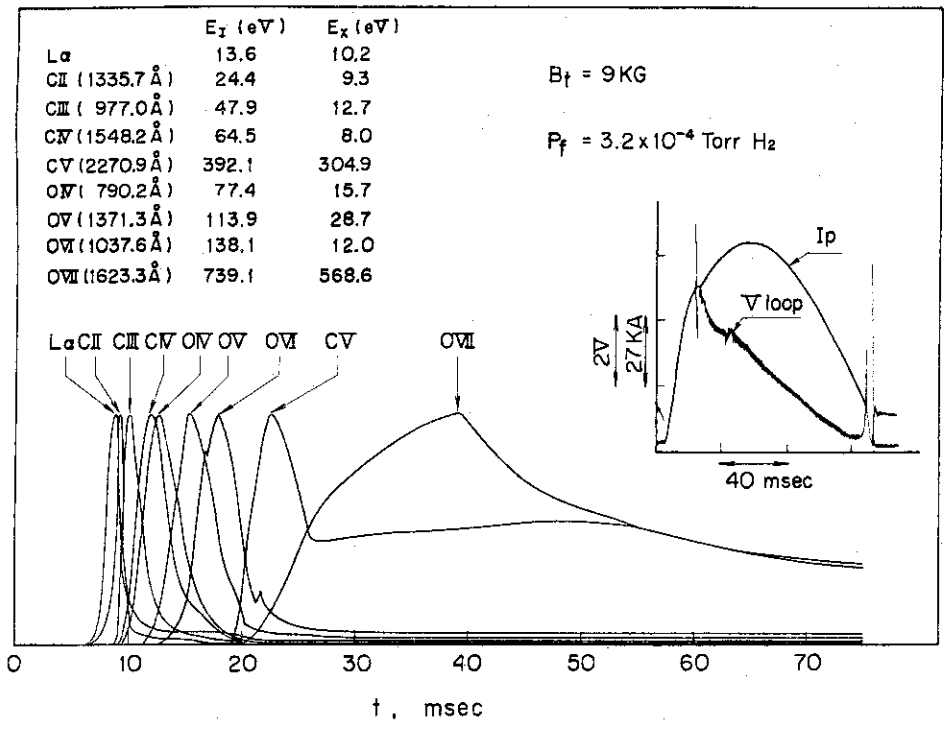

Fig. 7 Time-histories of intensities of different spectral lines.

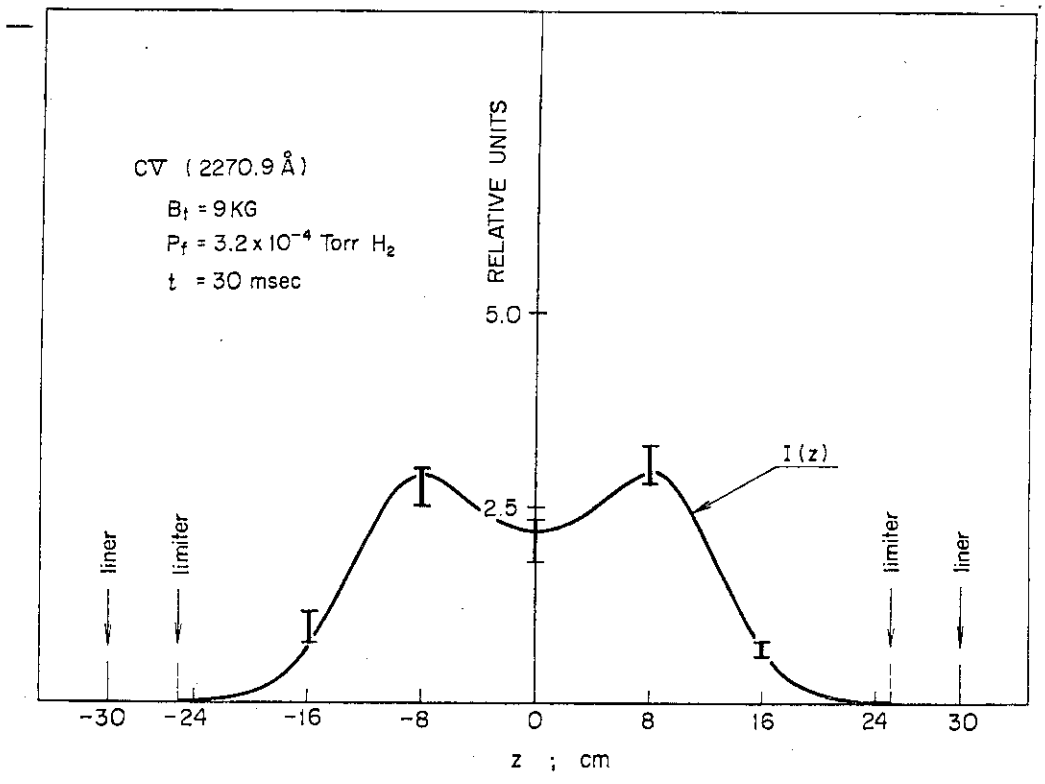

Fig. 8 Spatial distribution of spectral intensity for CV line at 30 msec.

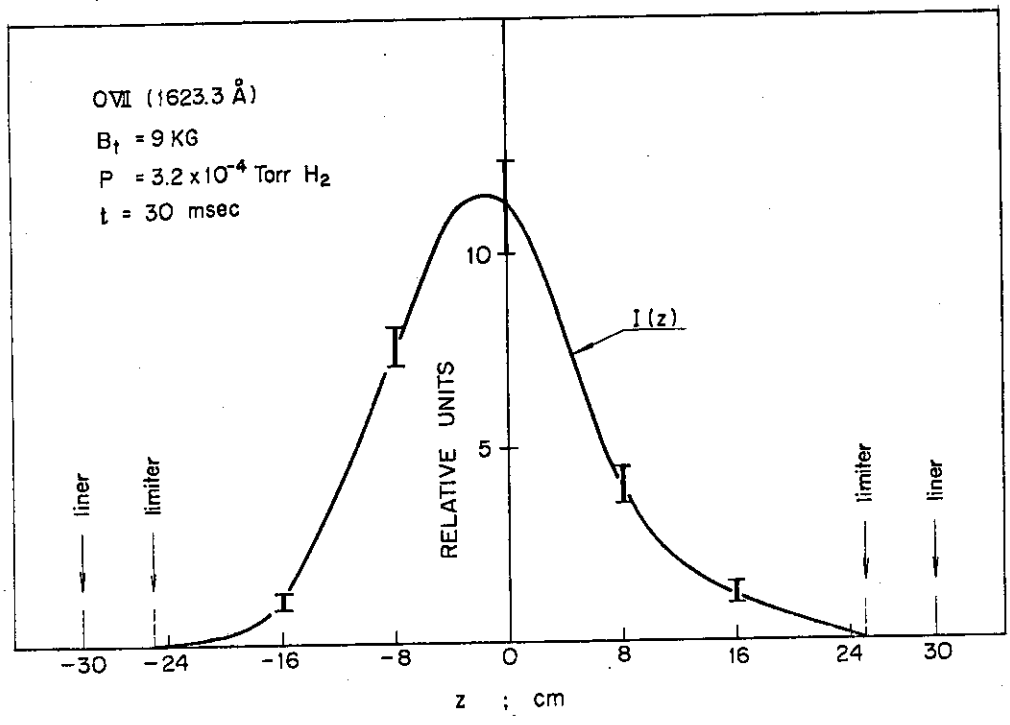

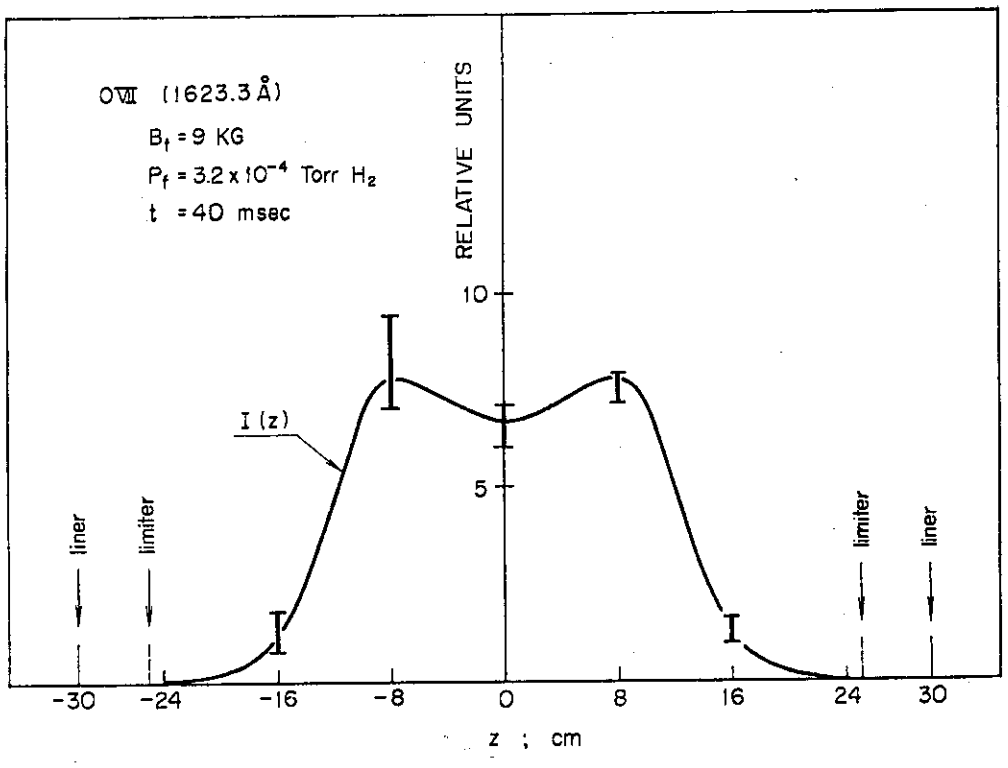

Fig. 9 Spatial distribution of spectral intensity for OVII line at 30 msec and 40 msec.

IV. RESULTS OF NUMERICAL CALCULATIONS

1. Coronal model, rate equations and spectral intensities

On numerical calculations for spectral lines emitted from impurities, the coronal model[21] is adopted. This model is sufficiently helpful to explain emissions from impurities and their ionization-states for hot tokamak plasmas. In the model the ionization and excitation processes are exclusively due to electron collisions and the radiative-recombination and radiative-decay processes are considered. The step-wise ionizations, excitations and cascade (three-body) recombinations and deexcitations are assumed to be neglected, and numbers of ions in excited levels are negligibly small compared with those in ground levels. Number densities of impurity ions in differently ionized states are determined by solving the following rate equations

$$\frac{dn_k}{dt} = n_e(\alpha_{k-1}n_{k-1} + \beta_{k+1}n_{k+1}) - n_e(\alpha_k n_k + \beta_k n_k) - n_k/\tau_k \quad , \qquad (1)$$

$$(k = 2, 3, \ldots\ldots, z+1)$$

where n_k represents the number density of ions with ionic charge (k-1), n_e electron density, τ_k confinement time, z atomic number of the impurity in question, α_{k-1} and α_k rate coefficients for collisional ionizations of ions with ionic charge (k-2) and (k-1) to the next ionization stages, and β_{k+1} and β_k radiative-recombination coefficients of ions with ionic charge (k) and (k-1) to the descending ionization stages. In the present analyses the contributions from dielectronic recombination processes[22-25] are not included. Equations on neutral atoms and fully-stripped ions are written by

$$\frac{dn_1}{dt} = n_e(\beta_2 n_2 - \alpha_1 n_1) + \phi \qquad (2)$$

and

$$\frac{dn_{z+1}}{dt} = n_e(\alpha_z n_z - \beta_{z+1}n_{z+1}) - \frac{n_{z+1}}{\tau_{z+1}} \qquad (3)$$

respectively. In Eq. (2) ϕ indicates a source term of impurity atoms outside the plasma, which is related to an influx ψ from walls of vacuum vessel or limiter by the following equation

$$\phi = \frac{2}{a}\psi \tag{4}$$

where ϕ and ψ are assumed to be uniform and a is the minor radius. Numerical expressions of α_k, β_k used in the present calculations are ones given by Hinnov[26] as

$$\alpha_k = 5.9\times10^{-8} q_k (E_k)^{-3/2} \sqrt{X_k}\, K_1(X_k) \tag{5}$$

and

$$\beta_k = 5.2\times10^{-14}(k-1)X_{k-1}^{3/2} e^{X_{k-1}} K_1(X_{k-1}) \ , \tag{6}$$

where E_k is the ionization potential (in Rydberg's unit of ions from the kth to (k+1)th state, X_k the ratio of ionization potential to electron temperature, $X_k = E_k I_H/T_e(eV)$ with $I_H = 13.6$ eV and q_k the number of equivalent electrons. And $K_1(X_k)$ is the exponential integral

$$K_1(X_k) = \int_{X_k}^{\infty} \frac{e^{-t}}{t}\, dt \tag{7}$$

The population in an excited level establishes itself in a time equal to the reciprocal of $\sum_{r<p} A(p,r)$ ($\sim10^{-8}$ sec except metastable levels), which is extremely short compared to variation-rates of electron temperature and density under experimental conditions in tokamak devices. Thus the population in the excited level can instantaneously follow the variations of temperature and density. The population density in the excited level is determined from a balance between a rate of collisional excitation directly from the ground level g to the excited level p and a rate of spontaneous radiative decay to its lower levels, i.e.,

$$n_e n_k(g) X_k(g,p) = n_k(p) \sum_{r<p} A(p,r) \tag{8}$$

where $n_k(g)$ and $n_k(p)$ represent ion densities in their ground levels and excited levels, respectively, and $A(p,r)$ is the spontaneous transition probability. $X_k(g,p)$ is the rate coefficient of collisional excitation from g-level to p-level and Seaton's expression[27] is here adopted, i.e.,

$$X_k(g,p) = \frac{7.89\times10^{-6}\,\bar{g}\, f_k}{T_e^{1/2} E_e} \exp\left(-\frac{E_e}{T_e}\right) . \tag{9}$$

In the equation E_e is the excitation potential in eV, $\bar{g}$ the effective

Gaunt-factor whose value is 0.2 for all different ionized ions and f_k the absorption oscillator strength. Values of $A(p,r)$ and f_k used in the present calculations are those given in the tables by Wiese et al.[28]

The intensity $I(p,q)$ of a spectral line arising from a transition between levels p and q is given by the following equation

$$I(p,q) = h\nu(p,q)n_k(p)A(p,q) \tag{10}$$

where $h\nu(p,q)$ is the photon energy corresponding to the transition. From Eqs. (8) and (10), the spectral intensity is expressed by

$$I(p,q) = h\nu(p,q)n_e n_k(g)X(g,p)\frac{A(p,q)}{\sum_{r<p} A(p,r)} \quad . \tag{11}$$

By combining Eqs. (1), (2), (3) with (11), time histories of intensities of spectral lines emitted from impurities can be obtained numerically.

2. Time-variation of electron temperature in the initial phase

We are going to discuss results of numerical calculations for time-histories of impurity lines obtained by using the model mentioned in the previous section and estimations of the time-variation of electron temperature in the initial phase of the JFT-2 plasma. Simultaneous differential equations (Eqs. (1), (2) and (3)) have been solved numerically by the Runge-Kutta-Gill method and time-histories of line intensities have been obtained from Eq. (11). In this section the plasma has been assumed to be uniform over a minor cross-section. The electron density and temperature have been respectively taken to be the experimental averaged one $\bar{n}_e(t)$ measured along the central microwave path and the averaged temperature defined as

$$\bar{T}_e = \int_0^a T_e(r)\cdot n_e(r)\cdot r dr \Big/ \int_0^a n_e(r)\cdot r dr \tag{12a}$$

with the minor radius a of the plasma column. If the profiles of electron temperature and density $T_e(r)$ and $n_e(r)$ are squared-distributions, Eq. (12a) becomes to

$$\bar{T}_e = \frac{2}{3} T_e(0) \quad . \tag{12b}$$

The central electron temperature $T_e(0)$ has been estimated by adjusting so

that the peak times for the different lines may coincide in the experimental and numerically-calculated cases.

The neutral light-impurities have been assumed to be uniformly distributed at the beginnings of the discharges. This assumption seems to be reasonable since deep penetrations into the plasmas of the impurities originating from desorptions at the vacuum wall are rather probable, at the beginnings of the discharges because of low densities. Thus initial conditions on the impurities have taken as follows;

$$n_1 = N_o \text{ (uniform in space)},$$
and
$$n_k = 0 \quad (k \neq 1) \ . \tag{13}$$

The amount of initial impurity has been taken to be $N_o = 1.6 \times 10^{11}$ cm^{-3} for oxygen and carbon atoms, which corresponds to one percent of the peak electron density. Successive impurity-influxes have been supposed to be neglected, i.e., $\psi(t) = \phi(t) = 0$. The confinement times τ_k have taken to be the same for all ionization stages, in a first approximation, i.e.,

$$\tau_k = \tau_p \ . \qquad (k = 2, 3, \ldots\ldots, z+1) \tag{14}$$

Numerical calculations have been performed for oxygen and carbon impurities and to the different confinement times (τ_p = infinite, 2 and 1 msec). Figure 10(a) shows time-histories for carbon (dotted curve) and oxygen ions (solid curve), which are calculated by putting τ_p infinite and by assuming a time-variation of electron temperature indicated by the dotted line of Fig. 11. The abrupt-rise of electron temperature at about 20 msec can reproduce a steeply-increasing slope on the CV line, which is observed experimentally. The arrows indicated in Fig. 10(a) provide the times when peak intensities of individual lines are observed for the JFT-2 plasma (see Fig. 7). In this case fairly good agreement between the calculations and the experiments is obtained on the times at peak intensities of spectral lines within about 1 msec. An introduction of τ_p-value results in some delay on peak intensities of individual lines. The delay is coming from the fact that a peak intensity is determined by the balance between the supply-rate of ions in the ionized state in question and the loss-rates due to ionizations, recombinations and diffusions across the magnetic field

(i.e., finite value of τ_p). Therefore, higher electron temperatures for finite τ_p than those for $\tau_p = \infty$ are required to give the times at peak intensities which accord experimental ones. The particle confinement times τ_H of proton are measured to be (5 -- 10) msec at (30 -- 40) msec[1,2] and to be equal to (1.5 -- 3.0) msec at 20 msec. Before 20 msec, the values of τ_H are thought to be (1 -- 2) msec. In the present paper the confinement time is assumed to be approximately the same for all plasma constituents: electrons, protons and the various impurity ions, as pointed out in ST-tokamak devices.[29] Figure 10(b) provides the time-histories calculated numerically for τ_p = 1 msec and an assumed time-variation of electron temperature is shown by the solid line in Fig. 11. In the figure are also shown the times when the experimental peaks are realized. In Fig. 10(b) the calculated peaks accord with the experimental ones within 1 or 2 msec before 20 msec. In the calculations peak intensities for CV and OVII lines are given at earlier times than the experimental ones, and their peak-times does not change significantly with variations of electron temperature. This discrepancy means that the value of τ_p = 1 msec may be too small to interpret these experimental peak-times. The peak-times for CV and OVII lines calculated from τ_p = 2 msec and assumed lower-temperature shown by the broken lines in the Fig. 11 are found to approach more the experimental ones within 1 msec and 5 msec, respectively.

The initial amount of neutral impurities has been substituted by a ten-times one, i.e., $N_o = 1.6 \times 10^{12}$ cm^{-3}. The numerical calculations for the value of N_o have not provided significantly changes of peak-times. The differences between these two peak-times are within 0.3 msec. The variations of 30 percents in the electron density from 10 to 20 msec have not almost changed the peak-times (within 0.3 msec). However, an introduction of source term ϕ* ranging from 10^{13} to 10^{16} cm^{-3} sec^{-1} has yielded slight delays in peak-times, which are corresponding to the temperature-rises of 20 eV.

From above-mentioned numerical results, it is possible to estimate the initial rise of central electron temperature which is shown in Fig. 12. The widths of these electron temperatures are originating from some ambiguity of τ_p-value. At 40 msec the central electron temperature has been (300 -- 350) eV, which is consistent of the results by measurements of ruby-laser scattering and soft X-ray spectra.[1] The open circles in the figure are referred to the values determined from the following equation;

---

* In conventional tokamaks, the value of ϕ is considered to be 10^{13} -- 10^{14} cm^{-3} sec^{-1}.[5]

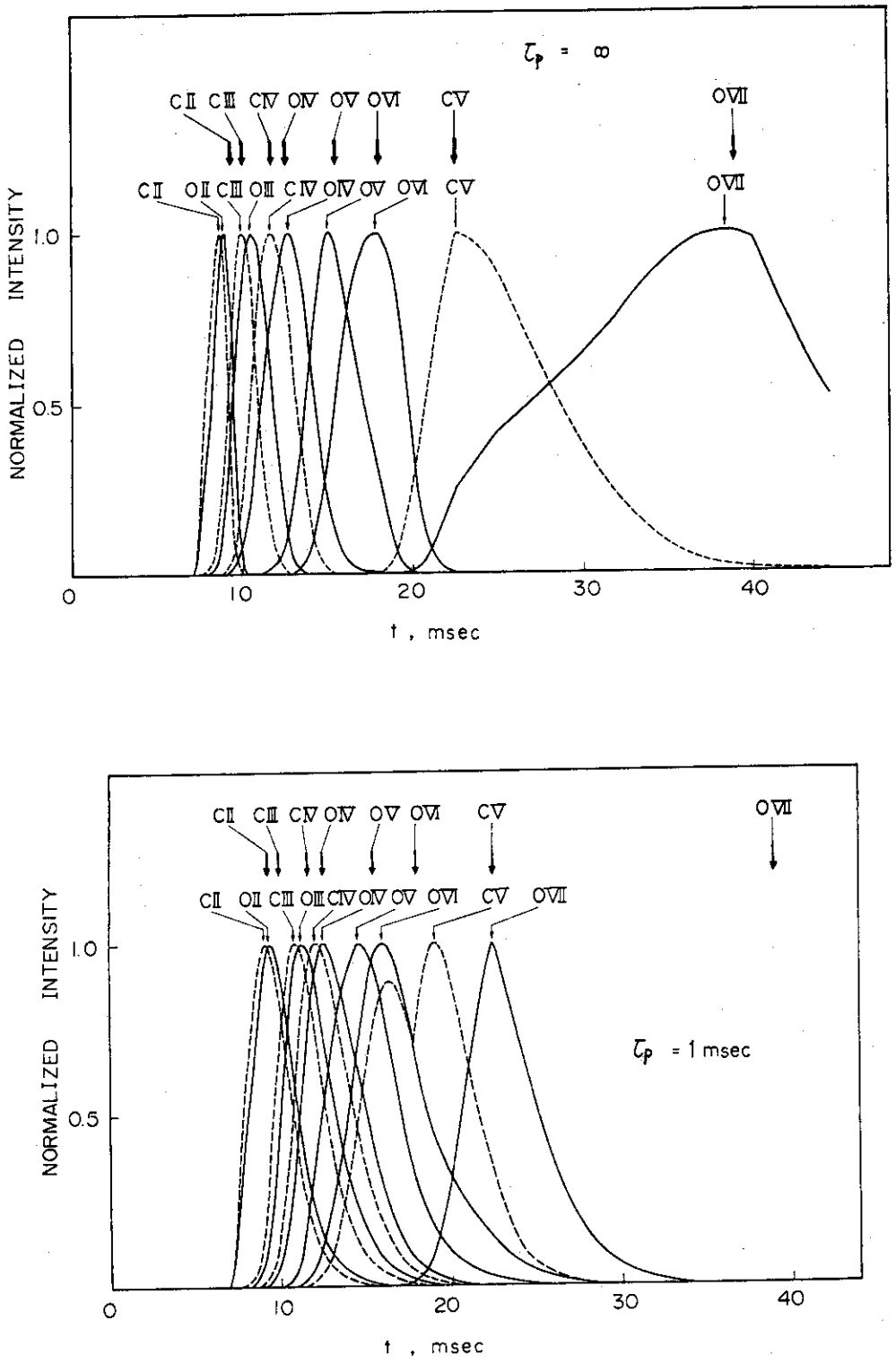

Fig.10 Time-histories calculated from time-variations of electron temperature indicated in Fig. 11 for $\tau_p = \infty$ (a) and $\tau_p = 1$ msec(b).

$$T_e(0) \simeq E_I \tag{15}$$

at the experimental peak-times of spectral lines except CV and CVII lines, whose ionization potentials are higher than the electron temperature at peak times of these lines. In the equation E_I is the ionization potential of the impurity-ions in question.

In Appendix of the present paper is given the computer program of numerical calculations used in this section.

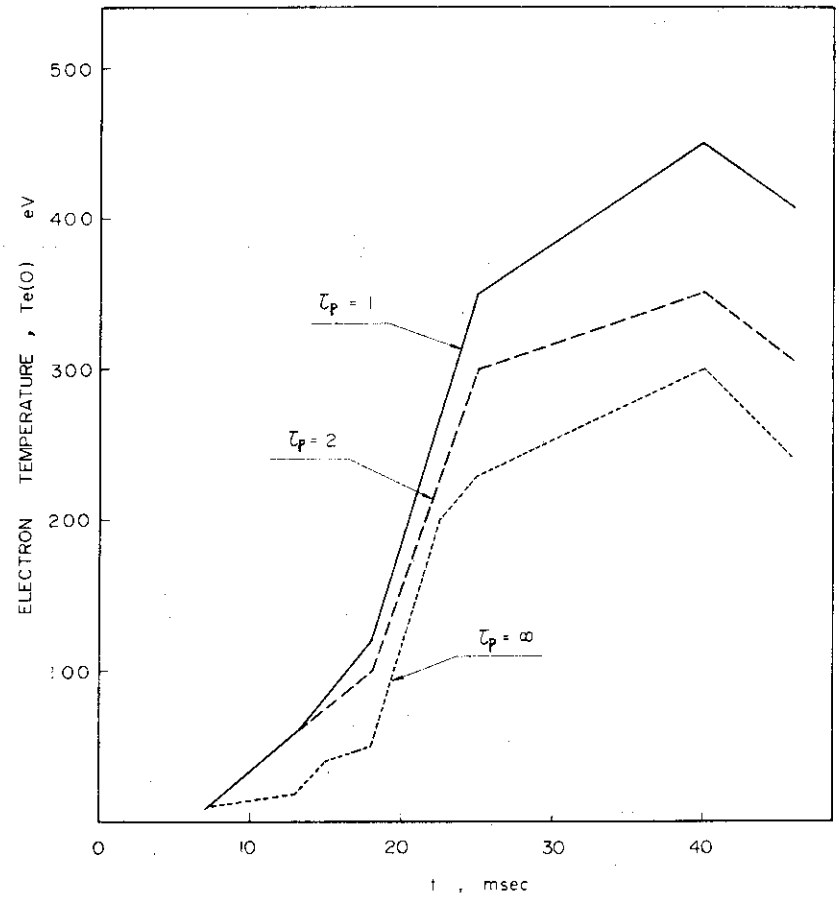

Fig.11 Assumed time-variations of central electron temperature.

3. Calculation on spatial distributions of spectral intensities

In this section distributions of spectral lines from impurity-ions are investigated numerically by taking into account the transportation of the ions which diffuse across the magnetic field and compared with experimental ones. Descriptions of the model used here are ones introduced by Tazima et al.[20] Under the assumption of axisymmetric-cylindrical approximation,

steady-state radial distributions+ of impurities in various ionized-states are expressed as follows;

$$-\frac{1}{r}\frac{d}{dr}(r\Gamma_k) + n_e(\alpha_{k-1}n_{k-1} + \beta_{k+1}n_{k+1}) - n_e(\alpha_k n_k + \beta_k n_k) = 0 \qquad (16)$$

with the boundary conditions;

$$\frac{dn_k}{dr} = 0 \qquad \text{at } r = 0 \text{ (on the axis)}$$

and (17)

$$n_k = 0 \qquad \text{at } r = a \text{ (on the plasma boundary).}$$

$$(k \neq 1)$$

The expressions of α_k and β_k are given in Section Ⅳ-1, and Γ_k is the diffusion flux across the magnetic field of impurity-ions in the (k-1)th ionized states.

The collisional frequency of impurity-ions in the (k-1)th ionized states with protons ν_k is given by

$$\nu_k = \frac{4\sqrt{2\pi}(k-1)^2 e^4 n_p \ell n\Lambda_k}{3\sqrt{m_p}(4\pi\varepsilon_o)^2 T_p^{3/2}} \frac{m_p}{m_z} \quad , \qquad (18)$$

where n_p, m_p and T_p are respectively the proton density, mass and temperature, $\ell n\Lambda_k$ is the Coulomb logarithm, m_z is the mass of impurity-ions, and e and ε_o are the well-known physical constants. It is found that ν_k is larger than

$$\nu^* = \frac{V_k}{Rq} \qquad (19)$$

with the thermal velocity of the impurity-ions V_k, the major radius R and the safety factor q. Therefore, in the present calculations it is reasonable to adopt the diffusion flux[12] deduced from the collisional MHD theory by assuming that the proton temperature equals to that of impurity-

---

+ Okamoto and Amano[30] have developed an impurity-evolution code which evaluates time-variations of radial distributions of impurity-ions.

ions and that effects on the gradient of the proton temperature is neglected, i.e.,

$$\Gamma_k = \Gamma_{PF} + \Gamma_{IN} \quad , \tag{20a}$$

$$\Gamma_{PF} = -D_{PF} \frac{dn_k}{dr} \quad , \tag{20b}$$

$$\Gamma_{IN} = D_{PF} \frac{k-1}{n_p} \frac{dn_p}{dr} n_k \quad , \tag{20c}$$

and

$$D_{PF} = \rho_k^2 \nu_k (1+q^2) \tag{20d}$$

$$(k = 2, 3, \ldots\ldots, z+1)$$

where D_{PF} is the Pfirsch-Schlüter diffusion coefficient and ρ_k Larmor radius of impurity-ion. The first term Γ_{PF} of Eq. (20a) indicates the diffusion flux due to the density gradient of impurity ions and the second term Γ_{IN} is the inward diffusion flux due to the density gradient of protons. And a radial distribution of neutral impurity is assumed to be expressed by a cylindrical model,

$$n_1(r) = \frac{n_1(a)}{4\pi} \int_0^{2\pi} d\phi \int_{-\pi/2}^{\pi/2} d\psi \cos\psi \exp\left[-\frac{1}{V_1} \int_{\rho_o}^{\rho_o} \alpha_1(\rho') n_e(\rho') d\rho'\right] \tag{21}$$

and the neutrals are supposed to enter the plasma at the mean thermal velocity V_1 of 5 eV.

Radial distributions of electron and proton temperatures and electron density at 30 msec used in numerical analyses are shown in Fig. 13. The central electron and proton temperatures are 300 and 100 eV, respectively. Figures 14(a) and (b) show the numerical results for CV and OVII lines at 30 msec. In the figures the abscissae indicate the vertical position Z and the ordinates are relative intensities integrated along the line of sight. Chain curves represented the spatial distributions numerically obtained from Eqs. (16), (17), (20) and (21). Impurity-ion flux Γ_k expressed by Eq. (20a) can not interpret the experimental distributions indicated by the solid lines. Thin and dotted curves show the results calculated by substituting 50 and 100 times of Γ_{PF} for the value given in Eq. (20b), respectively. The thin curve for CV can explain the position of peak intensity obtained experimentally within a spatial resolution (±3 cm) in measurements and the

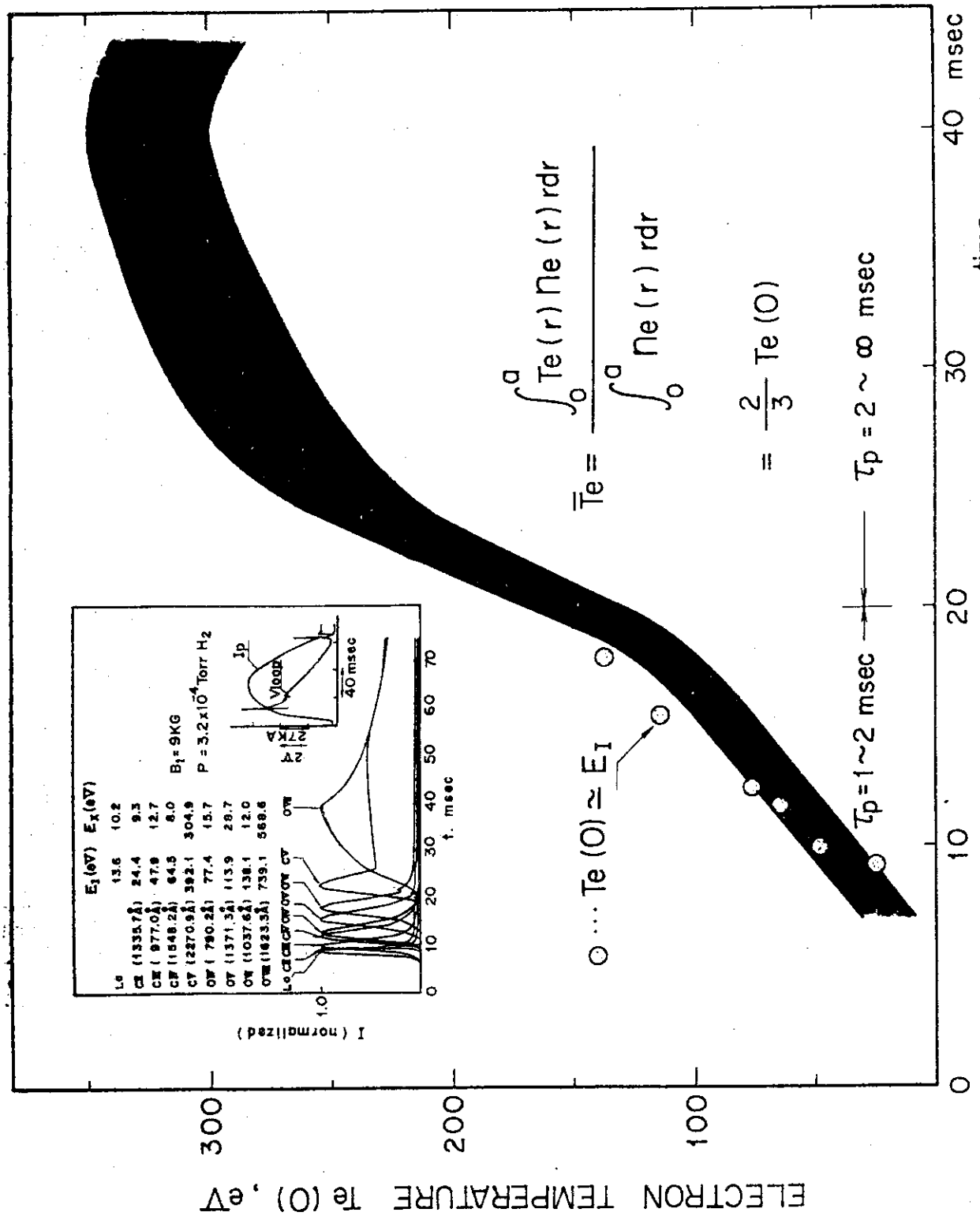

Fig.12 Initial rise of central electron temperature obtained from observed time-histories.

shell-type profiles. The distribution calculated from 50 × Γ_{PF} also fits well with the experimental one except the innor region of the column. For OVII lines the numerical peak-position calculated by substituting 50 or 100 times of Γ_{PF} also accords with the experimental result, and the numerical whole-shape approximately reproduces the experimental one which is a monotonously-decreasing function of the radius.

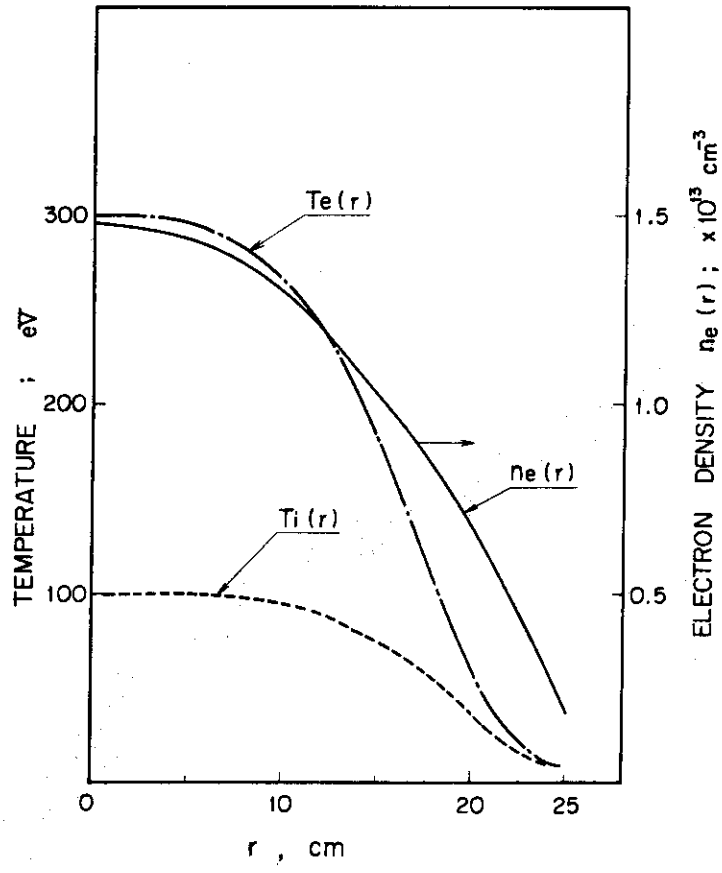

Fig.13 Radial distributions of electron and proton temperatures and electron density at 30 msec used in numerical analyses.

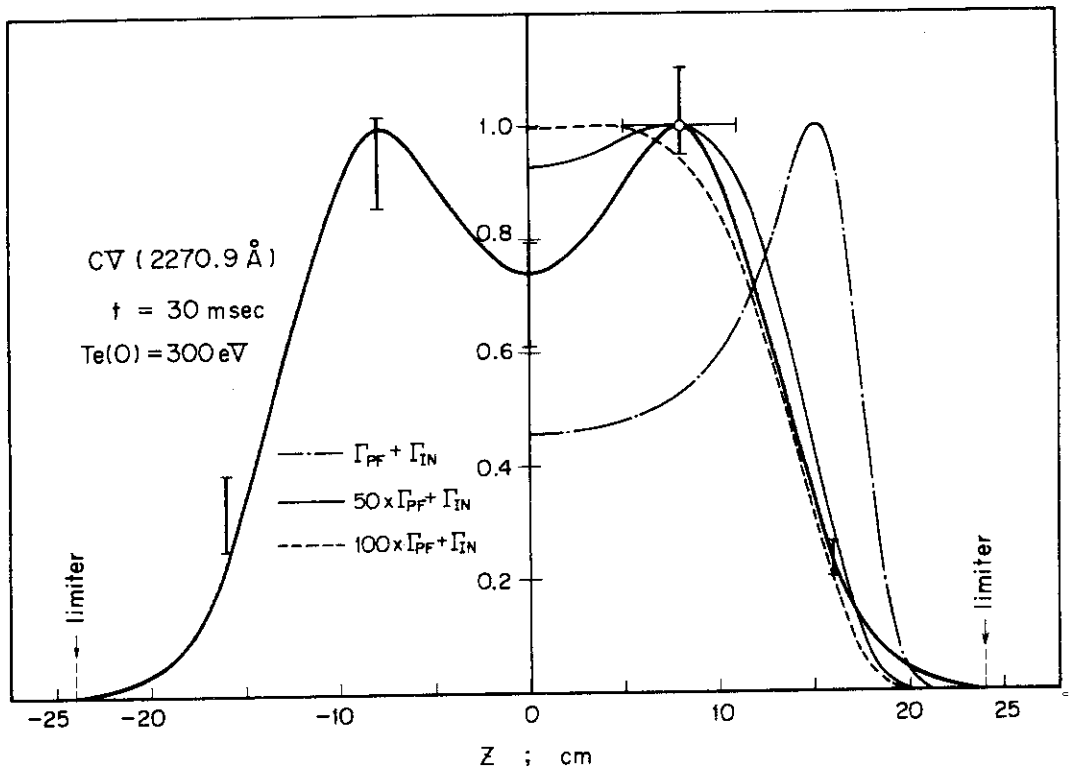

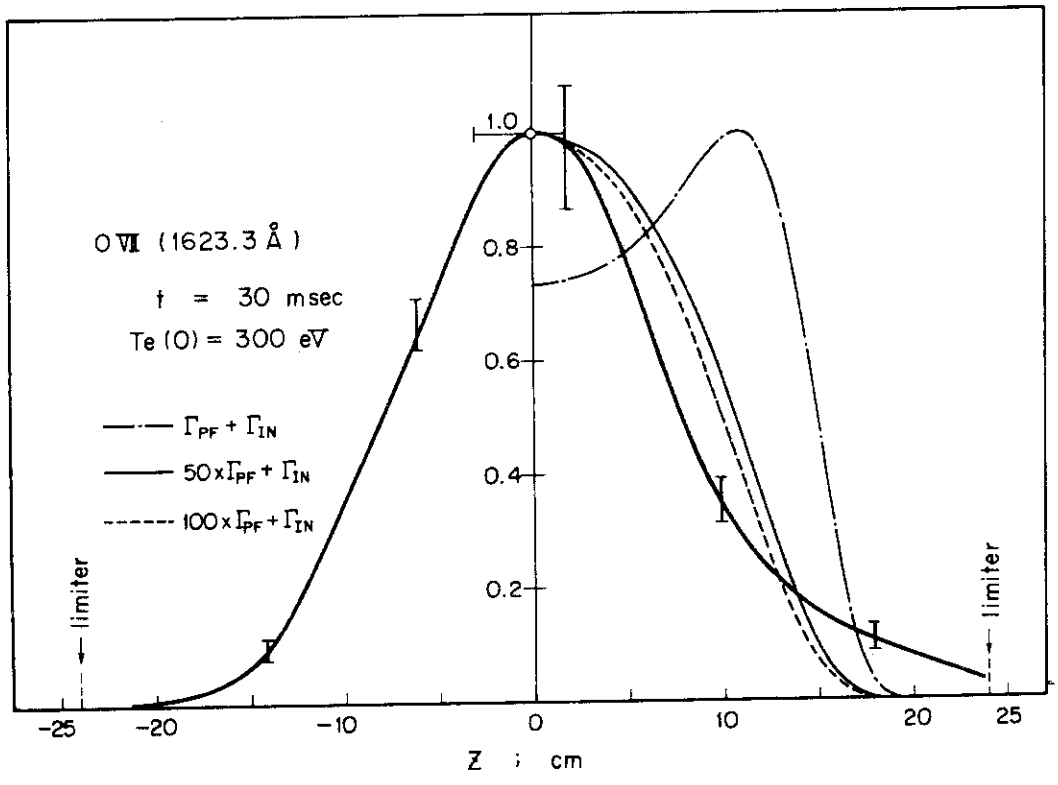

Fig.14 Calculated and experimental distributions of CV line(a) and OVII line(b).

V. DISCUSSION

Recently Cohen et al.[19] have investigated the transportation on aluminum-ions in the ATC device and compared experimental results with ones theoretically calculated considering the diffusion in the Pfirsch-Schlüter region, inward diffusion, ionization, and radiative and dielectronic recombinations. Their results have shown that the experimental profiles and peak positions for AlIX, AlX, and AXI were explained by numerical model including the Pfirsch-Schlüter and inward diffusion coefficients multiplied by factors of 10 and 2.5 respectively, but not by diffusion coefficients not multiplied by the factors. From these results they have concluded that the impurity-transportation in the ATC device was neoclassical (collisional) and included inward diffusion. In our numerical calculations where the Pfirsch-Schlüter and the inward diffusion-fluxes, ionization and radiative-recombination processes are taken into account, spatial distributions and the peak positions of CV and OVII lines are reasonably explained by the inward diffusion-flux and the diffusion-flux which is several ten times of Pfirsch-Schlüter's one.

VI. SUMMARY

We are summarizing the experimental and numerical results in the present paper in the following way.

(1) The time-histories of impurity-ion spectral lines and the spatial distributions of CV and OVII lines have been measured on a JFT-2 plasma under the condition; the toroidal magnetic field B_t = 9 kGauss and peak plasma current I_p = 76 kAmp.

(2) The intensity peak of spectral line emitted from the ion with the lower ionization-potential has appeared at the more early time and successively that with the higher ionization-potential has been observed.

(3) At 30 msec, the CV and OVII lines have peaked near r = 8 cm and the plasma center, respectively. At 40 msec, the peak position of the OVII line has observed near r = 8 cm.

(4) In numerical calculations for time-histories of impurity-lines higher electron temperatures for finite τ_p than those for $\tau_p = \infty$ have been required to give the times at peak intensity which have been accorded with experimental ones.

V. DISCUSSION

Recently Cohen et al.[19] have investigated the transportation on aluminum-ions in the ATC device and compared experimental results with ones theoretically calculated considering the diffusion in the Pfirsch-Schlüter region, inward diffusion, ionization, and radiative and dielectronic recombinations. Their results have shown that the experimental profiles and peak positions for AlIX, AlX, and AXI were explained by numerical model including the Pfirsch-Schlüter and inward diffusion coefficients multiplied by factors of 10 and 2.5 respectively, but not by diffusion coefficients not multiplied by the factors. From these results they have concluded that the impurity-transportation in the ATC device was neoclassical (collisional) and included inward diffusion. In our numerical calculations where the Pfirsch-Schlüter and the inward diffusion-fluxes, ionization and radiative-recombination processes are taken into account, spatial distributions and the peak positions of CV and OVII lines are reasonably explained by the inward diffusion-flux and the diffusion-flux which is several ten times of Pfirsch-Schlüter's one.

VI. SUMMARY

We are summarizing the experimental and numerical results in the present paper in the following way.

(1) The time-histories of impurity-ion spectral lines and the spatial distributions of CV and OVII lines have been measured on a JFT-2 plasma under the condition; the toroidal magnetic field B_t = 9 kGauss and peak plasma current I_p = 76 kAmp.

(2) The intensity peak of spectral line emitted from the ion with the lower ionization-potential has appeared at the more early time and successively that with the higher ionization-potential has been observed.

(3) At 30 msec, the CV and OVII lines have peaked near r = 8 cm and the plasma center, respectively. At 40 msec, the peak position of the OVII line has observed near r = 8 cm.

(4) In numerical calculations for time-histories of impurity-lines higher electron temperatures for finite τ_p than those for $\tau_p = \infty$ have been required to give the times at peak intensity which have been accorded with experimental ones.

(5) The numerical calculations for the value of the initial amount of neutral impurity, $N_o = 1.6 \times 10^{11}$ and 1.6×10^{12} cm^{-3} have not provided significantly changes of peak-times. The differences between these two peak-times have been within 0.3 msec.

(6) The variations of 30 percents in the electron density from 10 to 20 msec have not almost changed the peak-times within 0.3 msec.

(7) An introduction of source term ϕ ranging from 10^{13} to 10^{17} cm^{-3} sec^{-1} in numerical calculations for time-histories of impurity lines has yielded slight delays in peak-times, which have been corresponding to the temperature-rises of 20 eV.

(8) The initial rise of central electron temperature has been successfully estimated from observed time-histories of impurity-lines in the JFT-2 plasmas. The temperature at the peak-time has agreed with that given by

$$T_e(0) \simeq E_I$$

with the ionization potential E_I of impurity-ions in question. The central electron temperature at 40 msec has been (300 -- 350) eV, which has been consistent of the results by measurements of ruby-laser scattering and soft X-ray spectra.

(9) Impurity-ion flux determined by Pfirsch-Schluter and inward diffusions has not been able to interpret the experimental results. However, the distribution for CV line calculated from 50 times of Pfirsch-Schlüter and inward diffusion-fluxes has fitted well with the experimental result except the inner region of the column, and also the numerical whole-shape for OVII line has approximately reproduced the experimental one.

(10) The distributions calculated from (50 or 100) times of Pfirsch-Schlüter and inward diffusion-fluxes have explained the experimental ones more successfully than those calculated from only a few-hundred times of Pfirsch-Schlüter diffusion-flux.

ACKNOWLEDGEMENTS

The authors are very grateful to Drs. N. Fujisawa, T. Matoba, T. Shoji and other members of JFT-2 and diagnostic groups for their helpful discussions and co-operation, and to Mr. S. Kunieda and his crew for their operation of the JFT-2 device. We also greatly appreciate fruitful comments by Dr. K. Mori of the Institute of Physical and Chemical Research. We would like to express our gratitude to Drs. M. Tanaka and S. Mori for their continuous encouragement to the present work.

REFERENCES

1) N. Fujisawa et al.: Proceedings of the Fifth International Conference on Plasma Physics and Controlled Nuclear Fusion Research, November 1974, Tokyo (IAEA, Vienna, 1975) Vol.1, p.3.
2) A. Funahashi et al.: JAERI-M 5961 (January 1975).
3) L. M. Goldman and R. W. Kolb: Plasma Physics 6 (1964) 217.
4) G. D. Hobbs et al.: Proceedings of the Fifth International Conference on Ionization Phenomena in Gases, August 1961, Munich (North-Holland, Amsterdam, 1962) Vol.II, p. 1965.
5) TFR Group: Nuclear Fusion 15 (1975) 1053.
6) TFR Group: EUR-CEA-FC-777 (July 1975).
7) TFR Group: EUR-CEA-FC-783 (August 1975).
8) K. Ohasa et al.: to be published.
9) V. A. Vershkov and S. V. Mirnov: Nuclear Fusion 14 (1973) 383.
10) V. I. Gerrids and V. A. Krupin: MATT-TRANS 109 (1973), JETP Letters 18 (1973) 106.
11) J. W. Conner: Plasma Physics 15 (1973) 765.
12) T. Tsuda and M. Tanaka: JAERI-M 5376 (August 1973), J. Phys. Soc. Japan 38 (1975) 1228.
13) R. H. Rutherford: Phys. of Fluids 17 (1974) 1782.
14) E. Hinnov et al.: MATT-985 (December 1971), Plasma Physics 14 (1972) 755.
15) E. Hinnov: MATT-1022 (February 1974).
16) N. Bretz et al.: Proceedings of the Fifth International Conference on Plasma Physics and Controlled Nuclear Fusion Research, November 1974, Tokyo (IAEA, Vienna, 1975) Vol. 1, p.55, MATT-1077 (October 1974), Nuclear Fusion 15 (1975) 313.
17) S. von Goeler et al.: Nuclear Fusion 15 (1975) 301.

ACKNOWLEDGEMENTS

The authors are very grateful to Drs. N. Fujisawa, T. Matoba, T. Shoji and other members of JFT-2 and diagnostic groups for their helpful discussions and co-operation, and to Mr. S. Kunieda and his crew for their operation of the JFT-2 device. We also greatly appreciate fruitful comments by Dr. K. Mori of the Institute of Physical and Chemical Research. We would like to express our gratitude to Drs. M. Tanaka and S. Mori for their continuous encouragement to the present work.

REFERENCES

1) N. Fujisawa et al.: Proceedings of the Fifth International Conference on Plasma Physics and Controlled Nuclear Fusion Research, November 1974, Tokyo (IAEA, Vienna, 1975) Vol.1, p.3.
2) A. Funahashi et al.: JAERI-M 5961 (January 1975).
3) L. M. Goldman and R. W. Kolb: Plasma Physics 6 (1964) 217.
4) G. D. Hobbs et al.: Proceedings of the Fifth International Conference on Ionization Phenomena in Gases, August 1961, Munich (North-Holland, Amsterdam, 1962) Vol.II, p. 1965.
5) TFR Group: Nuclear Fusion 15 (1975) 1053.
6) TFR Group: EUR-CEA-FC-777 (July 1975).
7) TFR Group: EUR-CEA-FC-783 (August 1975).
8) K. Ohasa et al.: to be published.
9) V. A. Vershkov and S. V. Mirnov: Nuclear Fusion 14 (1973) 383.
10) V. I. Gerrids and V. A. Krupin: MATT-TRANS 109 (1973), JETP Letters 18 (1973) 106.
11) J. W. Conner: Plasma Physics 15 (1973) 765.
12) T. Tsuda and M. Tanaka: JAERI-M 5376 (August 1973), J. Phys. Soc. Japan 38 (1975) 1228.
13) R. H. Rutherford: Phys. of Fluids 17 (1974) 1782.
14) E. Hinnov et al.: MATT-985 (December 1971), Plasma Physics 14 (1972) 755.
15) E. Hinnov: MATT-1022 (February 1974).
16) N. Bretz et al.: Proceedings of the Fifth International Conference on Plasma Physics and Controlled Nuclear Fusion Research, November 1974, Tokyo (IAEA, Vienna, 1975) Vol. 1, p.55, MATT-1077 (October 1974), Nuclear Fusion 15 (1975) 313.
17) S. von Goeler et al.: Nuclear Fusion 15 (1975) 301.

18) TFR Group: Proceedings of the Fifth International Conference on Plasma Physics and Controlled Nuclear Fusion Research, November 1974, Tokyo (IAEA, Vienna, 1975) Vol.1, p.127.

19) S. A. Cohen et al.: MATT-1152 (October 1975).

20) T. Tazima et al.: JAERI-M 6606 (June 1976).

21) R. W. P. McWhirter: Spectral Intensities, in "Plasma Diagnostic Techniques" edited by R. H. Huddlestone and S. L. Leonard (Academic Press, New York and London, 1965) Chap. 5, p.201.

22) A. Burgess: Astrophys. J. 139 (1964) 776. 141 (1965) 1588.

23) H. P. Summers: Mon. Not. R. astr. Sco. 158 (1972) 255.

24) A. H. Gabriel and T. M. Paget: J. Phys. B. Atom. Molec. Phys. 5 (1972) 673.

25) T. P. Doanldson and N. J. Peacock: J. Quant. Spectrosc. Radiat. Transfer 16 (1976) 599.

26) E. Hinnov: MATT-777 (September 1970).

27) M. J. Seaton: The Theory of Excitation and Ionization by Electron Impact, in "Atomic and Molecular Processes" edited by D. R. Bates (Academic Press, New York and London, 1962) Chap. 11, p.374.

28) W. L. Wiese et al.: Atomic Transition Probabilities (National Bureau of Standards, Washington, 1966) Vol.1.

29) E. Hinnov: MATT-1240 (May 1976).

30) M. Okamoto and T. Amano: JAERI-M 6343 (December 1975).

Appendix

```
      C      TIME  HISTOLY  PROGRAM  OF  SPECTRAL  LINES
      C      RUNGE  KUTTA  GILL  METHOD
      C
     1        DIMENSION  X(200),ED(200),PI(20),PE(20),E@(20),OS(20),SC(20),AC(20
             1),EC(20),Y(20),@(20),F(20),INT(20),YNM(20),CONST(20),TE0(20),LL(20
             2),YY(20),TAUE(20),X1(20),X2(20),Y1(20),Y2(20)
     2        DIMENSION  TAUC(20),TAU0(20),TAM(20),T1(20),TAU1(20),T2(20),TAU2(2
             10)
     3        REAL  K1,K2,K3,K4,INT,INFLX
     4        DOUBLE PRECISION  KKS1,KKA1,XIS,XIA
      C
     5        READ (5,1500) INFLX
     6        READ (5,1600)  JJMAX
     7        READ (5,1601)  ( JJ,TAM(JJ),T1(JJ),TAU1(JJ),T2(JJ),TAU2(JJ),JJ=1,J
             1JMAX )
     8        READ (5,2000)  M,GAF
     9        READ (5,2100) H,JMAX,KMAX
    10        READ (5,3000)   ( YNM(J),X1(J),Y1(J),X2(J),Y2(J),J=1,JMAX )
    11        READ (5,4000)  ( PI(I),PE(I),OS(I),E@(I),I=2,M+2 )
    12        READ (5,5550) NN
    13        READ (5,5000) (X(N),ED(N),N=1,NN)
    14        READ (5,7000) (YY(K),LL(K),K=1,KMAX )
    15        READ (5,5555) YYE
    16   1500 FORMAT ( E12.4 )
    17   1600 FORMAT ( I6 )
    18   1601 FORMAT ( I6,5F6.2 )
    19   2000 FORMAT (I6,F10.4)
    20   2100 FORMAT (F10.4,I6,I6)
    21   3000 FORMAT ( 5F10.4 )
    22   4000 FORMAT( F10.4,F10.4,E12.4,F6.1 )
    23   5000 FORMAT (F12.4,E12.4)
    24   5550 FORMAT (I6)
    25   5555 FORMAT (F10.4)
    26   7000 FORMAT (F10.4,I6)
      C
    27        READ (5,6000) ( Y(I),I=1,M+2 )
    28   6000 FORMAT( 6E12.4 )
    29        SC(1)=0.0
    30        AC(1)=0.0
    31        EC(1)=0.0
    32        PI(1)=1.0
    33        PE(1)=1.0
    34        OS(1)=0.0
    35        E@(1)=0.0
    36        TAUE(1)=0.0
    37        I=M+2
    38        SC(I)=0.0
    39        AC(I+1)=0.0
    40        EC(I)=0.0
    41        TAUE(I)=0.0
    42        DO 8  JJ=1,JJMAX
    43        TAUC(JJ)= ( TAU1(JJ)-TAU2(JJ) )/( T1(JJ)-T2(JJ) )
    44        TAU0(JJ)=TAU1(JJ)-TAUC(JJ)*T1(JJ)
```

```
45        8 CONTINUE
46          DO 9  J=1,JMAX
47          CONST(J)=(Y1(J)-Y2(J))/(X1(J)-X2(J))
48          TE0(J)=Y1(J)-CONST(J)*X1(J)
49        9 CONTINUE
50          WRITE (6,2500) H,JMAX,KMAX
51          WRITE (6,3500) M,GAF
52          WRITE (6,1700)  INFLX
53          WRITE (6,3555)
54          WRITE (6,3550) ( J,YNM(J),CONST(J),TE0(J),X1(J),Y1(J),X2(J),Y2(J),
          1J=1,JMAX )
55          WRITE (6,4550)
56          WRITE (6,4500) ( I,PI(I),PE(I),OS(I),E@(I),Y(I),I=1,M+2 )
57          WRITE (6,6550)
58          WRITE (6,6500) ( X(N),ED(N),N=1,NN )
59          WRITE (6,7500)
60          WRITE (6,7550) ( K,YY(K),LL(K),K=1,KMAX )
61          WRITE (6,7555) YYE
62    2500 FORMAT (1H0,5X,12HHOSUU NO,H =,F10,4,10X,6HJMAX =,I6,10X,6HKMAX =,
          1I6/)
63    3500 FORMAT (1H ,5X,12H ATOM NO,M =,I6,14X,18HGAUNT FACTOR GAF =,F10,4/
          1/)
64    1700 FORMAT ( 1H ,5X,7HINFLX =,E12,4 / )
65    3555 FORMAT (1H0,10X,1HJ,4X,6HYNM(J),8X,8HCONST(J),11X,6HTE0(J),8X,5HX1
          1(J),10X,5HY1(J),10X,5HX2(J),10X,5HY2(J)//)
66    3550 FORMAT (1H ,5X,I6,F10,4,5X,F13,8,5X,F13,8,5X,F10,4,5X,F10,4,5X,F10
          1,4,5X,F10.4/)
67    4550 FORMAT (1H0,20X,1HI,6X,5HPI(I),10X,5HPE(I),11X,5HOS(I),8X,5HE@(I),
          110X,4HY(I)//)
68    4500 FORMAT (1H ,15X,I6,3X,F10,4,5X,F10,4,5X,E12,4,5X,F6,1,5X,E12,4/)
69    6550 FORMAT (1H ,5X,4HX(N),4X,5HED(N)//)
70    6500 FORMAT (1H ,5(5X,F4,1,E12,4,4X)/)
71    7500 FORMAT (1H0,20X,1HK,5X,5HYY(K),5X,5HLL(K)//)
72    7550 FORMAT (1H ,15X,I6,F10,4,2X,I6/)
73    7555 FORMAT (1H0,20X,5HYYE =,F10,4/)
74          DO 100  I=1,M+2
75          INT(I)=0,0
76     100 CONTINUE
77          Y(M+3)=0,0
78          J=1
79          JJ=1
80          DO 200  I=2,M+2
81          @(I)=0,0
82     200 CONTINUE
83          F(1)=1,0
84          CALL  TEMPE( TE,J,CONST,TE0,Y )
85          V=Y(1)
86          CALL  LAGS( X,ED,NN,V,EDL,ILL )
87          IF(ILL) 25,15,25
88       25 WRITE (6,300) ILL
89          GO TO 20
90       15 CONTINUE
91          EDL=1,0E+13*EDL
92          INFLX=INFLX/( 1,0E+13 )
93          Y(2)=Y(2)/( 1,0E+13 )
94          TAUI=TAUC(JJ)*Y(1)+TAU0(JJ)
95          CALL  RATEC( SC,AC,M,TE,PI,E@,TAUE,EDL )
```

```
      CALL  UHEN( F,M,EDL,SC,AC,Y,INFLX,TAUI )
      CALL  INTENS( EC,INT,M,GAF,OS,PE,TE,EDL,Y )
      CALL INSATU ( I,J,M,YNM,CONST,TE0,TE,EDL,SC,AC,EC,Y,F,INT,TAUE,TAU
      K=1
      L=1
   50 IF(Y(1)-YYE)  10,10,20
   10 IF(Y(1)-YNM(J)) 30,30,40
   40 J=J+1
   30 IF(Y(1)-TAM(JJ))  31,31,32
   32 JJ=JJ+1
C     RUNGE  KUTTA  GILL  LOOP  START
C
   31 DO 700  I=1,M+2
      K1=H*F(I)
      Q11=Q(I)
      R1=0.5*K1-Q11
      Q(I)=Q11+3.0*R1-0.5*K1
      Y(I)=Y(I)+R1
  700 CONTINUE
      CALL  TEMPE( TE,J,CONST,TE0,Y )
      V=Y(1)
      CALL  LAGS( X,ED,NN,V,EDL,ILL )
      IF(ILL) 55,45,55
   55 WRITE (6,300) ILL
      GO TO 20
   45 CONTINUE
      EDL=1.0E+13*EDL
      TAUI=TAUC(JJ)*Y(1)+TAU0(JJ)
      CALL  RATEC( SC,AC,M,TE,PI,EQ,TAUE,EDL )
      CALL  UHEN( F,M,EDL,SC,AC,Y,INFLX,TAUI )
      DO 800  I=1,M+2
      K2=H*F(I)
      Q12=Q(I)
      R2= (1-SQRT(0.5))*(K2-Q12)
      Q(I)=Q12+3.0*R2-(1-SQRT(0.5))*K2
      Y(I)=Y(I)+R2
  800 CONTINUE
      CALL  TEMPE( TE,J,CONST,TE0,Y )
      V=Y(1)
      CALL  LAGS( X,ED,NN,V,EDL,ILL )
      IF(ILL) 85,75,85
   85 WRITE (6,300) ILL
      GO TO 20
   75 CONTINUE
      EDL=1.0E+13*EDL
      TAUI=TAUC(JJ)*Y(1)+TAU0(JJ)
      CALL  RATEC( SC,AC,M,TE,PI,EQ,TAUE,EDL )
      CALL  UHEN( F,M,EDL,SC,AC,Y,INFLX,TAUI )
      DO 900  I=1,M+2
      K3=H*F(I)
      Q13=Q(I)
      R3=(1+SQRT(0.5))*(K3-Q13)
      Q(I)=Q13+3.0*R3-(1+SQRT(0.5))*K3
      Y(I)=Y(I)+R3
  900 CONTINUE
      CALL  TEMPE( TE,J,CONST,TE0,Y )
      V=Y(1)
```

```
151         CALL  LAGS( X,ED,NN,V,EDL,ILL )
152         IF(ILL) 205,105,205
153     205 WRITE (6,300) ILL
154         GO TO 20
155     105 CONTINUE
156         EDL=1.0E+13*EDL
157         TAUI=TAUC(JJ)*Y(1)+TAU0(JJ)
158         CALL  RATEC( SC,AC,M,TE,PI,EQ,TAUE,EDL )
159         CALL  UHEN( F,M,EDL,SC,AC,Y,INFLX,TAUI )
160         DO 1000  I=1,M+2
161         K4=H*F(I)
162         QI4=Q(I)
163         R4=( K4-2.0*QI4 )/6.0
164         Q(I)=QI4+3.0*R4-0.5*K4
165         Y(I)=Y(I)+R4
166    1000 CONTINUE
167         CALL  TEMPE( TE,J,CONST,TE0,Y )
168         V=Y(1)
169         CALL  LAGS( X,ED,NN,V,EDL,ILL )
170         IF(ILL) 505,405,505
171     505 WRITE (6,300) ILL
172         GO TO 20
173     405 CONTINUE
174         EDL=1.0E+13*EDL
175         TAUI=TAUC(JJ)*Y(1)+TAU0(JJ)
176         CALL  RATEC( SC,AC,M,TE,PI,EQ,TAUE,EDL )
177         CALL  UHEN( F,M,EDL,SC,AC,Y,INFLX,TAUI )
178         CALL  INTENS( EC,INT,M,GAF,OS,PE,TE,EDL,Y )
179         IF(Y(1)-YY(K)) 855,855,755
180     755 K=K+1
181         L=1
182     855 IF(L-LL(K)) 805,705,805
183     805 L=L+1
184         GO TO 905
185     705 CALL INSATU ( I,J,M,YNM,CONST,TE0,TE,EDL,SC,AC,EC,Y,F,INT,TAUE,TAU
           1I,INFLX )
186         L=1
187     905 GO TO 50
      C     KEISHIKI  SHITEI
      C
188     300 FORMAT (1H ,5HILL =,I6/)
189      20 STOP
190         END
```

```
      C     SUBROUTINE  PROGRAM  NO.1
      C     CALCULATION OF ELECTRON TEMPERATURE
      1     SUBROUTINE  TEMPE( TE,J,CONST,TE0,Y )
      2     DIMENSION  CONST(20),TE0(20),Y(20)
      3     TE=CONST(J)*Y(1)+TE0(J)
      4     TE=0.6666667*TE
      5     RETURN
      6     END
```

```
      C     SUBROUTINE  PROGRAM  NO.2
      C     CALCULATION OF IONIZATION AND RECOMBINATION RATE COEFFICIENT
      1     SUBROUTINE  RATEC( SC,AC,M,TE,PI,EQ,TAUE,EDL )
      2     DIMENSION  PI(20),EQ(20),SC(20),AC(20),TAUE(20)
      3     DOUBLE PRECISION  KKS1,KKA1,XIS,XIA
      4     DO 100  I=2,M+1
      5     XIS=PI(I)/TE
      6     XIA=PI(I-1)/TE
      7     CALL  DEXPI( KKS1,XIS,IERR )
      8     CALL  DEXPI( KKA1,XIA,IERR )
      9     SC(I)=(2.96E-6)*EQ(I)/(PI(I)**1.5)*DSQRT(XIS)*KKS1
     10     AC(I)=(5.2E-14)*(I-2)*(XIA**1.5)*DEXP(XIA)*KKA1
     11   100 CONTINUE
     12     I=M+2
     13     XIA=PI(I-1)/TE
     14     CALL  DEXPI( KKA1,XIA,IERR )
     15     AC(I)=(5.2E-14)*(I-2)*(XIA**1.5)*DEXP(XIA)*KKA1
     16     DO 200 I=2,M+1
     17     TAUE(I)=1.0/(SC(I)-AC(I+1))/EDL
     18   200 CONTINUE
     19     RETURN
     20     END
```

```
      C     SUBROUTINE  PROGRAM  NO.3
      C     KANSU  F  KEISAN
      C
      1     SUBROUTINE  UHEN( F,M,EDL,SC,AC,Y,INFLX,TAUI )
      2     DIMENSION  F(20),SC(20),AC(20),Y(20)
      3     REAL INFLX
      4     DO 100  I=2,M+1
      5     F(2)=1.0E-3*EDL*(AC(3)*Y(3)-Y(2)*SC(2))+INFLX
      6     F(I+1)=1.0E-3*EDL*(SC(I)*Y(I)+AC(I+2)*Y(I+2))-Y(I+1)*(SC(I+1)+AC(I
           1+1)) -Y(I+1)/TAUI
      7   100 CONTINUE
      8     RETURN
      9     END
```

```
      C      SUBROUTINE  PROGRAM  NO.4
      C      CALCULATION OF EXCITATION RATE COEFFICIENT AND SPECTRAL LINE
      C      INTENSITY
 1           SUBROUTINE  INTENS( EC,INT,M,GAF,OS,PE,TE,EDL,Y )
 2           DIMENSION  EC(20),INT(20),OS(20),PE(20),Y(20)
 3           REAL INT
 4           DO 100  I=2,M+1
 5           XE=PE(I)/TE
 6           EC(I)=(7.89E-6)*GAF*OS(I)/(SQRT(TE)*PE(I))/EXP(XE)
 7           INT(I)=EDL*Y(I)*EC(I)
 8           INT(I)= ( 1.0E+13 ) *INT(I)
 9       100 CONTINUE
10           RETURN
11           END



      C      SUBROUTINE NO.5
      C
      C    ---  COMPUTES THE EXPONENTIAL INTEGRAL          ---
      C    ---              IN THE RANGE  -4  TO  INFINITY  ---
      C
      C
 1           SUBROUTINE  DEXPI(ANS,X,IERR)
 2           DOUBLE PRECISION  X,ANS
 3           IERR = 0
 4           IF(X-4.D0) 10, 10, 20
 5       10  IF(X+4.D0) 55, 30, 30
      C
 6       20  ARG = 4.D0 / X
 7           ANS = DEXP(-X) * ((((((((.00094427614D0*ARG-.00493620070D0)*ARG
             *     +.01172327300)*ARG-.01755577900)*ARG+.02041209900)*ARG
             *     -.02295197900)*ARG+.03120856100)*ARG-.06249858800)*ARG
             *     +.24999999000)*ARG
 8           RETURN
      C
 9       30  IF(X) 40, 50, 40
      C
10       40  ANS = -DLOG(DABS(X))-((((((((((((.10317602D-11*X-.15798675D-10)*X
             *     +.16826592D-9)*X-.21915699D-8)*X+.27635830D-7)*X
             *     -.30726221D-6)*X+.30996040D-5)*X-.28337590D-4)*X
             *     +.23148392D-3)*X-.00166669060D0)*X+.01041666200)*X
             *     -.05555552000)*X+.25000000)*X-1.00000000)*X-.57721566000
11           RETURN
      C
12       50  ANS = 1.E75
13           RETURN
      C
14       55  IERR = 1
15           RETURN
16           END
```

```
      C      SUBROUTINE  PROGRAM  NO.6
      C      INSATU
      C
     1       SUBROUTINE  INSATU( I,J,M,YNM,CONST,TE0,TE,EDL,SC,AC,EC,Y,F,INT,TA
            1UE,TAUI,INFLX )
     2       DIMENSION  YNM(20),CONST(20),TE0(20),SC(20),AC(20),EC(20),Y(20),F(
            120),INT(20),TAUE(20)
     3       REAL  INT
     4       REAL  INFLX
     5       YT=7.0+Y(1)
     6       WRITE (6,100) YT  ,TE,EDL
     7       WRITE (6,101)  TAUI
     8       WRITE (6,102)  INFLX
     9       WRITE (6,200) YNM(J),CONST(J),TE0(J)
    10       WRITE (6,300)
    11       DO 8000  I=2,M+1
    12       YI= ( 1.0E+13 ) *Y(I)
    13       FI= ( 1.0E+13 ) *F(I)
    14       WRITE (6,400) I,SC(I),AC(I),EC(I),YI,FI,INT(I),TAUE(I)
    15    8000 CONTINUE
    16     100 FORMAT (1H0,7H TIME =,E12.4//6X,22HELECTRON TENPERATURE =,E10.3,7X
           1,16HELECTRON DENSITY =,E12.4/)
    17     101 FORMAT ( 1H ,6X,23HCONFINEMENT TIME TAUI =,F6.4 / )
    18     102 FORMAT ( 1H ,6X,7HINFLX =,E15.6 / )
    19     200 FORMAT (1H ,15X,8HYNM(J) =,F10.4,10X,10HCONST(J) =,F10.4,10X,8HTE0
           1(J) =,F10.4//)
    20     300 FORMAT (1H ,5X,1HI, 9X,5HSC(I),12X,5HAC(I),12X,5HEC(I),12X,4HY(I),
           113X,4HF(I),13X,6HINT(I),10X,7HTAUE(I)/)
    21     400 FORMAT (1H ,3X,I3,3X,E15.6,3X,E15.6,3X,E15.6,3X,E15.6,3X,E15.6,3X,
           1E15.6,3X,E15.6)
    22       RETURN
    23       END
```